Mathematical Biosciences 375 (2024) 109250

Contents lists available at ScienceDirect

Mathematical Biosciences

journal homepage: www.elsevier.com/locate/mbs

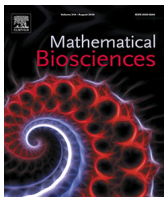

Original Research Article

Mathematical analysis of simple behavioral epidemic models

Leah LeJeune [a,b], Navid Ghaffarzadegan [c], Lauren M. Childs [a,b,1], Omar Saucedo [a,b,*,1]

[a] Department of Mathematics, Virginia Tech, 225 Stanger St, Blacksburg, 24061, USA
[b] Center for the Mathematics of Biosystems, Virginia Tech, Blacksburg, 24061, USA
[c] Department of Industrial and Systems Engineering, Virginia Tech, 7054 Haycock Rd, Falls Church, 22043, USA

ARTICLE INFO

Keywords:
Endogenous behavioral feedback
Identifiability
Human behavior
Stability analysis
Sensitivity analysis
Early COVID-19 dynamics

ABSTRACT

COVID-19 highlighted the importance of considering human behavior change when modeling disease dynamics. This led to developing various models that incorporate human behavior. Our objective is to contribute to an in-depth, mathematical examination of such models. Here, we consider a simple deterministic compartmental model with endogenous incorporation of human behavior (i.e., behavioral feedback) through transmission in a classic Susceptible–Exposed–Infectious–Recovered (SEIR) structure. Despite its simplicity, the SEIR structure with behavior (SEIRb) was shown to perform well in forecasting, especially compared to more complicated models. We contrast this model with an SEIR model that excludes endogenous incorporation of behavior. Both models assume permanent immunity to COVID-19, so we also consider a modification of the models which include waning immunity (SEIRS and SEIRSb). We perform equilibria, sensitivity, and identifiability analyses on all models and examine the fidelity of the models to replicate COVID-19 data across the United States. Endogenous incorporation of behavior significantly improves a model's ability to produce realistic outbreaks. While the two endogenous models are similar with respect to identifiability and sensitivity, the SEIRSb model, with the more accurate assumption of the waning immunity, strengthens the initial SEIRb model by allowing for the existence of an endemic equilibrium, a realistic feature of COVID-19 dynamics. When fitting the model to data, we further consider the addition of simple seasonality affecting disease transmission to highlight the explanatory power of the models.

1. Introduction

The COVID-19 pandemic left the world reeling, driving the need for further scientific understanding of disease dynamics, allowing for better preparedness for the next pandemic. Central to this preparedness is the ability to develop and implement policies which can mitigate the effects of the disease. To this end, mathematical models allow us to test and simulate the effects of potential policies [1]. One aspect of disease modeling that the recent pandemic brought to light was the strength of the impact of human behavior on disease dynamics. Along with policy implementation, human response affected the spread of the disease in massively different ways in different parts of the world [2,3]. Human behavior during disease outbreak manifests in a myriad of forms, including change in mobility, willingness to test for infection, willingness to vaccinate, adherence fatigue, and many others. One particular form of human behavior which was observed during the pandemic was the willingness of individuals to adopt and adhere to non-pharmaceutical interventions (NPIs), such as masking, social distancing, self-quarantining, even when not required to do so. Individuals tended to adhere to these interventions more strictly when perceived risk of infection was high, and individuals relaxed their adherence when perceived risk of infection was low, ultimately affecting disease spread [4]. Thus, considering change in human response over the course of a pandemic, as affected by changes in the state of the disease, is crucial for developing a better understanding of disease spread and constructing more effective policies.

A common model structure used in disease modeling is the deterministic, compartmental Susceptible–Infectious–Removed (SIR) ordinary differential equation (ODE) model [5–7]. In this model, the population is divided into three non-overlapping sub-populations based on disease status – Susceptible, Infectious, or Removed/Recovered – and the model simulates disease spread through these populations. The standard SIR model always indirectly makes assumptions on human behavior, particularly with respect to disease transmission. For example, through the ODE formulation, it inherently assumes a well-mixed population, and that human behavior remains unchanged throughout an epidemic [6]. While simple and easy to simulate, this is generally

* Corresponding author.
E-mail addresses: leahlejeune@vt.edu (L. LeJeune), navidg@vt.edu (N. Ghaffarzadegan), lchilds@vt.edu (L.M. Childs), osaucedo@vt.edu (O. Saucedo).
[1] These authors contributed equally.

https://doi.org/10.1016/j.mbs.2024.109250

Available online 14 July 2024

not how humans actually respond [8]. To relax this assumption, some SIR models instead assume that transmission changes through an external factor, e.g. as a function of time or some other measure [9,10]. However, human behavior instead tends to change in response to understanding of the state of the disease and changes in perceived risks ("risk perception") [4,11,12]. If risk perception is modeled internally, i.e. *endogenously*, a behavioral feedback mechanism emerges which is often referred to as a risk-response feedback loop, or human behavior adaptation [13]. The feedback loop couples change in the state of the disease with change in human behavior.

In recent years, and particularly in response to the COVID-19 pandemic, modelers attempted to account for human behavior in order to forecast future disease outbreaks [14]. However, not all models considered human behavior changes occurring internal to the model. Those without internal changes due to human behavior, referred to as *exogenous* models [15], lacked predictive power [4]. Other models incorporated human behavior endogenously in various ways. Model types and methods include network and agent-based models [16–19], game theory and optimization [20–23], opinion dynamics [24–26], and deterministic compartmental models [4,27,28]. Explored in several reviews articles [13,14,29–31], some of these models allow for endogenously driven disease waves. In particular, the systematic review by Hamilton et al. [31] characterized models which included endogenous human behavior (taking a variety of forms — masking, social distancing, vaccination, etc.) either as feedback loops, game theory/utility theory, and information/opinion spread. The vast majority of these models used feedback loops and compartmental models. Overall, the review concluded that endogenous incorporation of human behavior in infectious disease models could aid in better prediction of outcomes, allowing for better epidemic preparedness and response [31].

A recent review study from our group focuses on models incorporating human behavior in the form of risk response in deterministic, compartmental models [32]. The study pointed to a particular SIR-type model (defined below), developed by Rahmandad and colleagues [4], for its simplicity and ability to outperform a significant portion of remarkably more complex models. Rahmandad et al.'s model is an extension of the aforementioned SIR model, considering a latent population (E), which includes individuals who are infected but are not yet infectious. Furthermore, the model takes the standard constant transmission (usually denoted as β) and reconstructs it as a function of either prevalence, deaths, perceived prevalence, or perceived deaths. This results in the endogenous SEIRb (b for behavior) model. The model's considerable forecasting performance was mainly due to the endogenous consideration of human behavior changes occurring in response to changes in disease dynamics [4]. Recent studies examined various policy or practical insights emerging from the SEIRb model [33,34].

In this paper, we provide an in-depth analysis of the mathematical properties of epidemic models incorporating human behavior. These models are simple in structure, not taking into account the impact of mobility, vaccinations, or outbreaks occurring from new strains. Specifically we explore the mathematical structure of the SEIRb model to further understand the driving factors of its forecasting strength. We primarily compare two versions of the model: one which considers permanent immunity (SEIRb) and one which considers waning immunity (SEIRSb) and also observe key differences between these endogenous models and their well-studied exogenous counterparts (SEIR and SEIRS). In Section 2, we introduce the SEIRb and SEIRSb models, including definitions for the variables and parameters. To help with further analyses, we scale the system to a total population size of one. In Section 3, we perform equilibria and identifiability analyses on the models as well as determine the basic reproductive number. In Section 4, we assess the sensitivity of the infectious population to the parameters. We also compare numerical simulations of the models and validate models by fitting them to COVID-19 data across a wide range of regions covering different US states and districts, and over multiple waves of the pandemic. Finally, in Section 5, we summarize our findings and their implications.

Table 1
State variables and parameters for SEIRb model, found in System (1), and SEIRSb model, found in System (3).

Variables	
S	Population of susceptible individuals
E	Population of exposed (and infected) individuals
I	Population of infectious individuals
R	Population of recovered individuals
F	Number of perceived/lagged infections
Parameters	
β	Base transmission rate
α	Sensitivity to (risk of) infection
γ	(infection) risk diminishing impact
N	Total population size ($N = S + E + I + R$)
τ_E	Exposure period, average time in state E
τ_I	Infectious period, average time in state I
τ_F	Time lag between infections awareness and actual infection occurrence
τ_R[a]	Period of immunity, average time in state R

[a] Only appears in System (3).

2. Models

We consider two simple models incorporating endogenous human behavior feedback: one with permanent immunity, SEIRb, and one with waning immunity, SEIRSb. Both models build upon an underlying SEIR framework with susceptible (S), exposed (E), infectious (I) and recovered (R) individuals. All variables and parameters for these models are described in Table 1.

The models we developed primarily focus on the impact of human behavior on transmission. More specifically, this is assumed to represent the adherence of individuals to NPIs, where the level of adherence is a result of perceived risk of infection. The type of NPI used to reduce transmission can represent many actions — from social distancing and self-isolation to masking or reducing mobility. From a biological perspective, these are all distinct; however, mathematically, these are equivalent in the SEIRb/SEIRSb model as they ultimately result in reduction of transmission when implemented. Choosing a specific type of NPI to model, such as social distancing, may need to be employed differently if additional complexities exist in the model, such as the inclusion of age structure. Given the general nature of the SEIRb structure from [4], the model can represent multiple NPIs, any of which result in the reduction of transmission.

2.1. Epidemic model with permanent immunity: SEIRb

We begin by considering the SEIRb model with permanent immunity, given by

$$\begin{aligned}
\frac{dS}{dt} &= -\frac{\beta}{(1+\alpha F)^{\gamma}} S \frac{I}{N}, \\
\frac{dE}{dt} &= \frac{\beta}{(1+\alpha F)^{\gamma}} S \frac{I}{N} - \frac{E}{\tau_E}, \\
\frac{dI}{dt} &= \frac{E}{\tau_E} - \frac{I}{\tau_I}, \\
\frac{dR}{dt} &= \frac{I}{\tau_I}, \\
\frac{dF}{dt} &= \frac{I-F}{\tau_F}.
\end{aligned} \tag{1}$$

In addition to the four state variables in the standard SEIR model, there is an additional state variable, F, the number of perceived infections, which is how risk perception is incorporated. The state variable F is a simple exponential first-order delay of I, modulated by the difference between perceived prevalence (F) and actual prevalence (I). In addition, compared to the standard SEIR model, this model incorporates a transmission function in terms of the state variable F, $\beta(F) = \frac{\beta}{(1+\alpha F)^{\gamma}}$, rather than simply using a constant parameter (often β). These two key

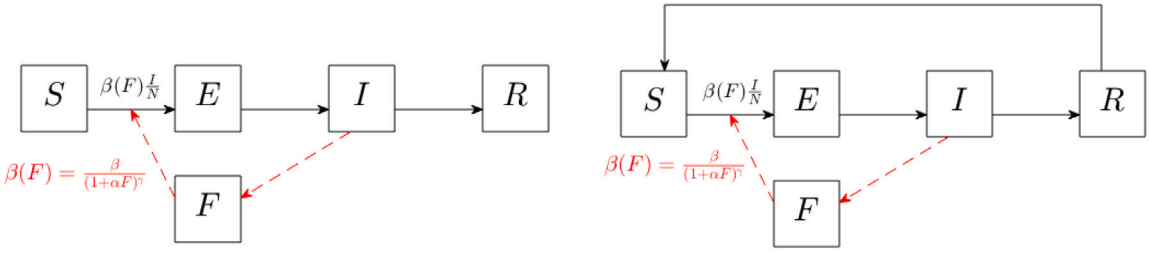

(a) Permanent immunity (SEIRb) model (b) Waning immunity (SEIRSb) model

Fig. 1. Flow diagram describing the general structure of the SEIRSb model. Red dashed lines indicate influences on disease transmission. Solid black lines denote movement of individuals. The compartments are S, susceptible; E, exposed; I, infectious; R, removed; F, perceived/lagged infectious.

components are essential to the realistic epidemic dynamics this model can produce.

The incorporation of risk perception drives the appearance of multiple waves in simulations on the time scale of an epidemic (see Section 4), a feature missing in models which consider transmission as constant or a function of factors external to the model [32]. In a steady state, $I = F$, so $\frac{dF}{dt} = 0$ and F remains constant. Perturbing the system with an increase in I, such that $I > F$, results in $\frac{dF}{dt}$ becoming positive, increasing F, and lowering $\beta(F)$. As $\beta(F)$ declines enough (such that $\frac{dE}{dt} < 0$), the size of E declines as well, which leads to $\frac{dI}{dt} < 0$ and a decrease in I. Once $I < F$, $\frac{dF}{dt}$ becomes negative, F declines, and in turn, $\beta(F)$ increases. This mechanism is known as a *negative feedback loop* (see Fig. 1) and is the central feature of the model's predictive power.

The formulation of risk perception in the transmission term can take multiple forms [35–37]. We choose our transmission function as a modification from Rahmandad et al. [4], who consider that deaths/perceived deaths, as a function of prevalence/perceived prevalence, drive transmission dynamics. For the sake of simplicity, we assume transmission is driven by prevalence/perceived prevalence. Compared to the transmission term in [4], the changes made involve exclusion of the seasonality term w (considered again during model validation in Section 4) and a re-scaling of F in the final equation, which does not qualitatively impact overall model dynamics.

For generalizability and to avoid losing model dynamics in the magnitude difference between total population size N and the relatively small size of the latent, infectious, and recovered populations, we re-scale the model. Letting $a = \alpha N$ and

$$s = \frac{S}{N},\ e = \frac{E}{N},\ i = \frac{I}{N},\ r = \frac{R}{N},\ f = \frac{F}{N},$$

gives the normalized SEIRb system

$$\begin{aligned}
\frac{ds}{dt} &= -\frac{\beta}{(1+af)^\gamma} si, \\
\frac{de}{dt} &= \frac{\beta}{(1+af)^\gamma} si - \frac{e}{\tau_E}, \\
\frac{di}{dt} &= \frac{e}{\tau_E} - \frac{i}{\tau_I}, \\
\frac{dr}{dt} &= \frac{i}{\tau_I}, \\
\frac{df}{dt} &= \frac{i-f}{\tau_F}.
\end{aligned} \tag{2}$$

The corresponding exogenous (SEIR) system can be found in Appendix A in Eq. (A.1). Compared to the SEIRb model in Eq. (2), the SEIR model has constant transmission: β rather than $\beta(f)$. As a result, the equation for perceived infections, f, is no longer necessary.

2.2. Simple epidemic model with waning immunity: SEIRSb

Waning immunity creates an additional pathway between the recovered (R) and susceptible (S) compartments with a flow of $\frac{R}{\tau_R}$. Thus, the revised system of ODEs has much the same structure as System (1) except the first and fourth compartments are changed by the addition and subtraction of waning immunity term $\frac{R}{\tau_R}$, respectively, to form

$$\begin{aligned}
\frac{dS}{dt} &= -\frac{\beta}{(1+\alpha F)^\gamma} S\frac{I}{N} + \frac{R}{\tau_R}, \\
\frac{dE}{dt} &= \frac{\beta}{(1+\alpha F)^\gamma} S\frac{I}{N} - \frac{E}{\tau_E}, \\
\frac{dI}{dt} &= \frac{E}{\tau_E} - \frac{I}{\tau_I}, \\
\frac{dR}{dt} &= \frac{I}{\tau_I} - \frac{R}{\tau_R}, \\
\frac{dF}{dt} &= \frac{I-F}{\tau_F}.
\end{aligned} \tag{3}$$

With the same rescaling as for System (1), we obtain the normalized SEIRSb system

$$\begin{aligned}
\frac{ds}{dt} &= -\frac{\beta}{(1+af)^\gamma} si + \frac{r}{\tau_R}, \\
\frac{de}{dt} &= \frac{\beta}{(1+af)^\gamma} si - \frac{e}{\tau_E}, \\
\frac{di}{dt} &= \frac{e}{\tau_E} - \frac{i}{\tau_I}, \\
\frac{dr}{dt} &= \frac{i}{\tau_I} - \frac{r}{\tau_R}, \\
\frac{df}{dt} &= \frac{i-f}{\tau_F}.
\end{aligned} \tag{4}$$

The corresponding exogenous (SEIRS) system can be found in Appendix A in Eq. (A.2). Compared to the standard model in Eq. (4), the SEIRS model has constant transmission: β rather than $\beta(f)$, such that the equation for perceived infections, f, is also no longer necessary.

3. Theory and calculation

3.1. Equilibrium analysis

We begin our analysis by deriving the various equilibria for both models (SEIRb and SEIRSb), giving conditions on existence and uniqueness. For completeness, we summarize the equilibria for corresponding exogenous models (SEIR and SEIRS) in Appendix A.

Theorem 1. *Disease free equilibria.*

Given biologically relevant parameters, i.e., $\{\beta, a, \gamma, \tau_E, \tau_I, \tau_F, \tau_R\} > 0$, *and biologically realistic initial conditions, i.e.,* $\{s(0), e(0), i(0), r(0), f(0)\} \in [0, 1]$,

1. *the permanent immunity (SEIRb) model, found in System (2), has a line of disease free equilibria given by* $\bar{s} = 1 - \bar{r}$, *where the precise value of the equilibrium depends on the initial condition.*
2. *the waning immunity model (SEIRSb) model, found in System (4), has a unique disease free equilibrium (DFE)* $(1, 0, 0, 0, 0)$.

Proof. First, notice that both models are closed with respect to movement of individuals, and thus the following relationship holds:

$$s(t) + e(t) + i(t) + r(t) = 1. \tag{5}$$

Item (1) follows from Eq. (5) combined with the fact that $\frac{dr}{dt} = 0$ results in $\bar{i} = 0$; thus, with $\frac{di}{dt} = 0$, this results in $\bar{e} = \bar{i} = 0$, with no requirements on the values of $\bar{s}$ and $\bar{r}$. As $\frac{df}{dt} = 0$ and $\bar{i} = 0$, $\bar{f} = 0$. Item (2) follows from Eq. (5) and the fact that $\frac{di}{dt} = \frac{dr}{dt} = 0$ results in $\bar{e} = \bar{i} = \bar{r} = 0$. As $\frac{df}{dt} = 0$ and $\bar{i} = 0$, $\bar{f} = 0$. □

We derive the basic reproduction number $\mathcal{R}_0$ (the number of secondary infections produced by a single infectious individual in a fully susceptible population). For the permanent immunity model, $\mathcal{R}_0$ gives information about initial disease dynamics (whether the infectious population grows or declines), but the disease always dies out. For the waning immunity model, $\mathcal{R}_0$ gives information about conditions driving the disease to extinction [38]. In both cases, we use the next-generation method [39] to derive $\mathcal{R}_0$ using the *e-i* infectious subsystem. We calculate the Jacobian J of the *e-i* subsystem evaluated at the equilibrium $(\bar{s}, \bar{e}, \bar{i}, \bar{r}, \bar{f})$ as

$$J = \begin{pmatrix} -\frac{1}{\tau_E} & \frac{\beta}{(1+a\bar{i})^\gamma}\bar{s} \\ \frac{1}{\tau_E} & -\frac{1}{\tau_I} \end{pmatrix}.$$

In the case of permanent immunity, where we have infinitely many DFE, the basic reproduction number is calculated using the DFE $(1, 0, 0, 0, 0)$, i.e. the DFE where no outbreak has occurred. Thus, $\bar{s} = 1$ and $\bar{e} = \bar{i} = \bar{r} = \bar{f} = 0$ in the calculation of $\mathcal{R}_0$ for both models, resulting in

$$J\Big|_{(\bar{s}=1,\bar{e}=0,\bar{i}=0,\bar{r}=0,\bar{f}=0)} = \begin{pmatrix} -\frac{1}{\tau_E} & \beta \\ \frac{1}{\tau_E} & -\frac{1}{\tau_I} \end{pmatrix}.$$

Splitting apart into a matrix of new infections and a matrix of transitions between states, we write $J = F - V$ with

$$F = \begin{pmatrix} 0 & \beta \\ 0 & 0 \end{pmatrix}, \quad V = \begin{pmatrix} \frac{1}{\tau_E} & 0 \\ -\frac{1}{\tau_E} & \frac{1}{\tau_I} \end{pmatrix}.$$

The basic reproduction number $\mathcal{R}_0$ is the spectral radius of FV^{-1}, i.e. the eigenvalue with largest real part (in magnitude), given by

$$FV^{-1} = \begin{pmatrix} \tau_I\beta & \tau_I\beta \\ 0 & 0 \end{pmatrix}.$$

Thus,

$$\mathcal{R}_0 = \beta\tau_I,$$

for both the permanent immunity (SEIRb) model and the waning immunity (SEIRSb) model.

For the latter model, as the DFE is unique, the DFE will be locally asymptotically stable when $\mathcal{R}_0 < 1$ and unstable when $\mathcal{R}_0 > 1$ [39–41].

In the case of permanent immunity, System (2), the only equilibria present are the line of disease free equilibrium. No endemic equilibria can exist since the susceptible compartment only contains a decay function and no growth. Thus, eventually the susceptible population will become too small to sustain the disease. In the case of waning immunity, the additional pathway between recovered and susceptible allows for a richer set of equilibria, i.e. the existence of an endemic equilibria.

Theorem 2. *Endemic equilibrium for SEIRSb model.*

Given biologically relevant parameters, i.e., $\{\beta, a, \gamma, \tau_E, \tau_I, \tau_F, \tau_R\} > 0$, *and biologically realistic initial conditions, i.e.,* $\{s(0), e(0), i(0), r(0), f(0)\} \in [0, 1]$, *there exists a unique endemic equilibrium (EE) for System (4) if and only if* $\mathcal{R}_0 > 1$.

Proof. Using System (4), we write all compartments in terms of $\bar{i}$:

$$\bar{s} = \frac{(1+a\bar{i})^\gamma}{\beta\tau_I}, \ \bar{e} = \frac{\tau_E}{\tau_I}\bar{i}, \ \bar{r} = \frac{\tau_R}{\tau_I}\bar{i}, \ \bar{f} = \bar{i}.$$

Using Eq. (5), with the equations above, results in

$$(a\bar{i}+1)^\gamma + \beta(\tau_E + \tau_I + \tau_R)\bar{i} - \beta\tau_I = 0,$$

which we rewrite as

$$(1+a\bar{i})^\gamma = \beta\tau_I - \beta(\tau_E + \tau_I + \tau_R)\bar{i}. \tag{6}$$

Given the assumption that all parameters are positive (consistent with the biologically relevant region), then the left hand side of Eq. (6) is increasing monotonically from 1 as $\bar{i}$ increases and the right hand side in decreasing linearly from $\beta\tau_I$ as $\bar{i}$ increases. When $\mathcal{R}_0 = \beta\tau_I > 1$, these two curves will intersect at exactly one point in the positive quadrant, indicating a unique EE. When $\mathcal{R}_0 = \beta\tau_I < 1$, these two curves will not intersect in the positive quadrant, and thus there will be no endemic equilibrium in the biologically relevant region. When $\beta\tau_I$ exactly equals one, these two curves will intersect exactly at one, when $\bar{i} = 0$. This is equivalent to the DFE, and hence the EE does not exist when $\mathcal{R}_0 \leq 1$. □

For the SEIRSb model, as the DFE becomes unstable when $\mathcal{R}_0 > 1$ and there is a unique EE, we expect this EE to be stable. However, due to our implicit solution of the EE, we can only numerically show that the EE is stable for $\mathcal{R}_0 > 1$. For example, using LHS sampling across a wide range of biologically realistic parameters, where $\mathcal{R}_0 > 1$, always yields negative eigenvalues for the Jacobian evaluated at the EE. We include the Jacobian matrix, evaluated at the EE, below:

$$J\Big|_{\left(\frac{(1+a\bar{i})^\gamma}{\beta\tau_i}, \frac{\tau_E}{\tau_I}\bar{i}, \frac{\tau_R}{\tau_I}\bar{i}, \frac{\tau_R}{\tau_I}\bar{i}\right)} = \begin{pmatrix} -\frac{\beta}{(1+a\bar{i})^\gamma}\bar{i} - \frac{1}{\tau_R} & -\frac{1}{\tau_R} & -\frac{1}{\tau_I} - \frac{1}{\tau_R} & \frac{a\gamma}{(1+a\bar{i})\tau_I}\bar{i} \\ \frac{\beta}{(1+a\bar{i})^\gamma}\bar{i} & -\frac{1}{\tau_E} & \frac{1}{\tau_I} & -\frac{a\gamma}{(1+a\bar{i})\tau_I}\bar{i} \\ 0 & \frac{1}{\tau_E} & -\frac{1}{\tau_I} & 0 \\ 0 & 0 & \frac{1}{\tau_F} & -\frac{1}{\tau_F} \end{pmatrix},$$

where $\bar{i}$ is the solution to Eq. (6). While it is possible to derive a condition for the local asymptotic stability of the EE using the Routh–Hurwitz Criteria, it is not obviously associated with $\mathcal{R}_0$ and is too algebraically complex to be useful for determining stability (except numerically).

We summarize the results from this section in Table 2.

3.2. Identifiability analysis

An important aspect of model development is the parameterization of the system. Often a model is parameterized by searching through the literature for viable parameter values. Another popular approach for parameterization is to use a fitting procedure such as least squares to fit the model to observable data. When fitting to data, one must verify if the model structure is formulated in a way that allows for the model parameters to be uniquely identified given perfectly observed data. We refer to this process as structural identifiability [42–44]. Mathematically, we say that a model is *globally structurally identifiable* for the set of parameters $\mathbf{p_1}$ if for every parameter set $\mathbf{p_2}$, the relationship $y(t, \mathbf{p_1}) = y(t, \mathbf{p_2})$ implies $\mathbf{p_1} = \mathbf{p_2}$. If there is a neighborhood in which the equation above holds true, we say the model is *locally identifiable*. A model is classified as *unidentifiable* if the definitions above are not met. Assessing the structural identifiability of a model provides insights on the practical identifiability of a model by determining whether it is possible given any amount of data to recover the model parameters. A parameter that is deemed structurally unidentifiable can lead to inaccurate estimates when using numerical methods, which is why it is crucial to conduct structural identifiability first. The practical identifiability

Table 2
Equilibria for SEIRb model, found in System (2), and SEIRSb model, found in System (4), assuming biologically relevant parameters, i.e., $\{\beta, a, \gamma, \tau_E, \tau_I, \tau_F, \tau_R\} > 0$, and biologically realistic initial conditions, i.e., $\{s(0), e(0), i(0), r(0), f(0)\} \in [0, 1]$.

Model	Equilibrium type	Values	Existence, uniqueness, and stability
SEIRb	Disease free (DFE)	$(\bar{s}, 0, 0, \bar{r}, 0)$, $\bar{s} + \bar{r} = 1$	There always exists a line of DFE.
SEIRSb	Disease free (DFE)	$(1, 0, 0, 0, 0)$	Always exists and is a unique DFE Locally asymptotically stable when $\mathcal{R}_0 < 1$ Unstable when $\mathcal{R}_0 > 1$
	Endemic (EE)	$\left(\frac{A}{\mathcal{R}_0}, \frac{\tau_E}{\tau_I}\bar{i}, \bar{i}, \frac{\tau_R}{\tau_I}\bar{i}, \frac{\tau_R}{\tau_I}\bar{i}, \bar{i}\right)$, $\bar{i} \in (0, 1)$, $A := (1 + a\bar{i})^\gamma$	Exists and is a unique, stable[a] EE when $\mathcal{R}_0 > 1$ Does not exist when $\mathcal{R}_0 \leq 1$

[a] As described in the text, the stability condition is determined numerically.

of a model can be determined by implementing several methodologies such as the Monte Carlo algorithm [45], Likelihood Profiles [46], and Sensitivity Analysis [34]. In this manuscript, we focus on conducting the structural identifiability of SEIRb and SEIRSb models. In particular, we focus our efforts on output measures, e.g. prevalence or number of deaths data. Identifiability for the analogous exogenous models (SEIR and SEIRS) are found in Appendix B. Although we do not conduct practical identifiability in this manuscript, the results that we attain from structural identifiability will guide our future work by informing which parameters we should target and what type of data we will need when we perform practical identifiability.

There exist an array of user friendly and powerful software that test the structural identifiability of models [47]. For this paper, we use the Julia package *StructuralIdentifiability.jl* developed by Dong et al. [48]. *StructuralIdentifiability.jl* is an open-access package that uses a differential algebra approach to assess the identifiability properties of a model by describing the input–output equations via projections. The software also provides informative metrics such as functions for identifiable state variables and model parameters, and it has the ability to assess local identifiability.

3.2.1. Permanent immunity: SEIRb

For tractability, we focus on integer values of γ (in particular, $\gamma = 1, 2, 3, 4, 5$) such that the denominator of the function β is a polynomial. With these restrictions, the SEIRb model with all initial conditions for state variables known and unknown parameters is globally identifiable (Theorem 3). When the initial conditions for the state variables and model parameters are unknown, the SEIRb model is globally identifiable for a, β, and τ_F and locally identifiable for τ_E and τ_I (Theorem 4). For completeness, we summarize results of identifiability analysis for corresponding exogenous models (SEIR and SEIRS) in Appendix B.

Theorem 3. *Identifiability of SEIRb model with initial conditions.*

The SEIRb model given by System (2) is globally structurally identifiable when all initial conditions for the state variables are known, the model parameters are unknown, and prevalence (size of class i) is the output measure.

Proof. Define the parameters sets $\mathbf{p}_1 = \{a, \beta, \tau_F, \tau_I, \tau_E\}$ and $\mathbf{p}_2 = \{\hat{a}, \hat{\beta}, \hat{\tau_F}, \hat{\tau_I}, \hat{\tau_E}\}$. Let $y(t, \mathbf{p}_1) = y(t, \mathbf{p}_2)$. Then we obtain the following functional relationships from *StructuralIdentifiability.jl*:

$$a = \hat{a}, \quad \beta = \hat{\beta}, \quad \tau_F = \hat{\tau}_F, \quad \tau_I = \hat{\tau}_I, \quad \tau_E = \hat{\tau}_E.$$

Thus, $\mathbf{p}_1 = \mathbf{p}_2$ which entails that the SEIRb model is globally structurally identifiable with respect to prevalence data. □

Theorem 4. *Identifiability of SEIRb model without initial conditions.*

The SEIRb model (2) is locally structurally identifiable when initial conditions for the state variables are unknown, the model parameters are unknown, and prevalence (size of class i) is the output measure. In particular, τ_F and τ_I are locally identifiable while a, β, τ_F are globally identifiable.

Table 3
Identifiability of SEIRb and SEIRSb models for $\gamma \in \{1, 2, 3, 4, 5\}$ using Julia package.

Model	γ	Globally Identifiable	Locally Identifiable	Unidentifiable
SEIRb	1	a, β, τ_F	τ_E, τ_I	
	2	a, β, τ_F	τ_E, τ_I	
	3	a, β, τ_F	τ_E, τ_I	
	4	a, β, τ_F	τ_E, τ_I	
	5	a, β, τ_F	τ_E, τ_I	
SEIRSb	1	a, β, τ_F, τ_R	τ_E, τ_I	
	2	a, β, τ_F, τ_R	τ_E, τ_I	
	3	*	*	*
	4	*	*	*
	5	*	*	*

* Indicates the software ran out of memory when performing the computation.

Proof. As in the proof for Theorem 4, define the parameters sets $\mathbf{p}_1 = \{a, \beta, \tau_F, \tau_I, \tau_E\}$ and $\mathbf{p}_2 = \{\hat{a}, \hat{\beta}, \hat{\tau}_F, \hat{\tau}_I, \hat{\tau}_E\}$. Let $y(t, \mathbf{p}_1) = y(t, \mathbf{p}_2)$. Then, we obtain the following functional relationships from *StructuralIdentifiability.jl*:

$$a = \hat{a}, \quad \beta = \hat{\beta}, \quad \tau_F = \hat{\tau}_F, \quad \tau_I\tau_E = \hat{\tau}_I\hat{\tau}_E, \quad \tau_E + \tau_I = \hat{\tau}_E + \hat{\tau}_I. \tag{7}$$

Solving the System (7) using *Mathematica*, we obtain two set of solutions:

$$\{a = \hat{a},\ \beta = \hat{\beta},\ \tau_I = \hat{\tau}_E,\ \tau_E = \hat{\tau}_I,\ \tau_F = \hat{\tau}_F\},$$
$$\{a = \hat{a},\ \beta = \hat{\beta},\ \tau_I = \hat{\tau}_I,\ \tau_E = \hat{\tau}_E,\ \tau_F = \hat{\tau}_F\}. \tag{8}$$

From the set of solutions in (8), we conclude that the SEIRb model is locally identifiable. □

3.2.2. Waning immunity: SEIRSb

As with the SEIRb model, for tractability purposes, we focus on integer values of γ. For $\gamma = 1, 2, 3$ the SEIRSb model with known initial conditions for the state variables and model parameters is globally identifiable (Theorem 5). With unknown initial conditions for the state variables and unknown model parameters, the SEIRSb is globally identifiable for a, β, τ_F, and τ_R and locally identifiable for τ_E and τ_I (Theorem 6). The software ran out of memory performing the computation for $\gamma = 3, 4, 5$ so no identifiability could be determined (see Table 3).

Theorem 5. *Identifiability of SEIRSb model with initial conditions.*

The SEIRSb model given by System (4) is globally identifiable when all initial conditions for the state variables are known and prevalence (size of class i) is the output measure.

Proof. Let $\mathbf{p}_1 = \{a, \beta, \tau_F, \tau_I, \tau_E, \tau_R\}$ and $\mathbf{p}_2 = \{\hat{a}, \hat{\beta}, \hat{\tau_F}, \hat{\tau_I}, \hat{\tau_E}, \hat{\tau}_R\}$. Suppose that $y(t, \mathbf{p}_1) = y(t, \mathbf{p}_2)$. Then we obtain the following functional relationships from *StructuralIdentifiability.jl*:

$$a = \hat{a}, \quad \beta = \hat{\beta}, \quad \tau_F = \hat{\tau}_F, \quad \tau_I = \hat{\tau}_I, \quad \tau_E = \hat{\tau}_E, \quad \tau_R = \hat{\tau}_R.$$

Hence, $\mathbf{p}_1 = \mathbf{p}_2$. This means that the SEIRSb model is globally structurally identifiable with respect to prevalence data. □

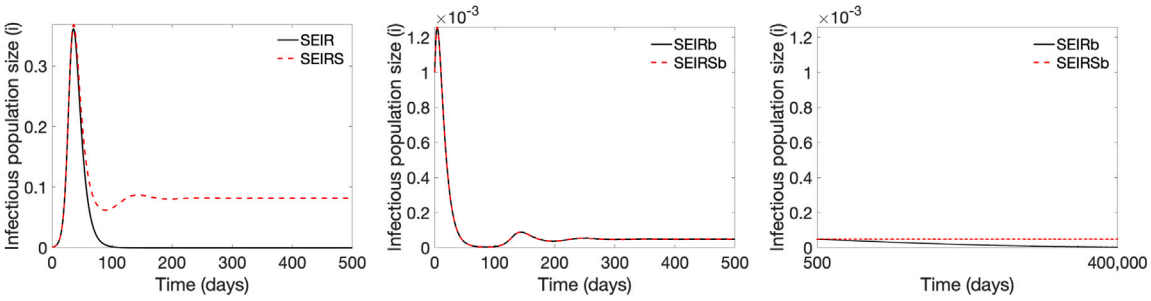

(a) Dynamics (without behavior) (b) Initial dynamics (with behavior) (c) Long-term dynamics (with behavior)

Fig. 2. Comparison of dynamics of the infectious populations. Initial conditions for susceptible, exposed, and infectious populations differ here from Table 4 in order to observe differing model dynamics in a shorter time frame: $s(0) = 1 - 0.002$; $e(0) = 0.001$; $i(0) = 0.001$. Figure (a) Dynamics of the exogenous models, which clearly differ for the SEIR and SEIRS models. (b) Initial and (c) long-term dynamics of the outbreak of the SEIRb and SEIRSb models.

Theorem 6. *Identifiability of SEIRSb model without initial conditions.*

The SEIRSb model (4) is locally structurally identifiable when the state variables are unknown, the model parameters are unknown, and prevalence (size of class i) is the output measure. In particular, τ_F and τ_I are locally identifiable while a, β, τ_F, τ_R are globally identifiable.

Proof. Once more, define the parameters sets $\mathbf{p}_1 = \{a, \beta, \tau_F, \tau_I, \tau_E, \tau_R\}$ and $\mathbf{p}_2 = \{\hat{a}, \hat{\beta}, \hat{\tau}_F, \hat{\tau}_I, \hat{\tau}_E, \hat{\tau}_R\}$. Let $y(t, \mathbf{p}_1) = y(t, \mathbf{p}_2)$. Using *StructuralIdentifiability.jl*, we attain the functional relationships:

$$a = \hat{a}, \quad \beta = \hat{\beta}, \quad \tau_F = \hat{\tau}_F, \quad \tau_R = \hat{\tau}_R, \quad \tau_I\tau_E = \hat{\tau}_I\hat{\tau}_E, \quad \tau_E + \tau_I = \hat{\tau}_E + \hat{\tau}_I. \tag{9}$$

Solving the System (9) using *Mathematica*, we generate two set of solutions:

$$\{a = \hat{a},\ \beta = \hat{\beta},\ \tau_I = \hat{\tau}_E,\ \tau_E = \hat{\tau}_I,\ \tau_F = \hat{\tau}_F,\ \tau_R = \hat{\tau}_R\},$$
$$\{a = \hat{a},\ \beta = \hat{\beta},\ \tau_I = \hat{\tau}_I,\ \tau_E = \hat{\tau}_E,\ \tau_F = \hat{\tau}_F,\ \tau_R = \hat{\tau}_R\}. \tag{10}$$

The set of solutions in (10) imply that SEIRSb model is locally identifiable. □

4. Results and discussion

4.1. Numerical simulations

To show the time-varying dynamics of our model systems, we numerically simulate all models, found in Systems (2), (A.1), (4), and (A.2), in Matlab 2019a (time-varying sensitivity analysis and numerical simulations) and 2024a (global sensitivity analysis) using the `ode45` solver with the `NonNegative` flag for all equations. Table 4 gives initial conditions and parameter values used in simulations, unless otherwise specified.

Fig. 2 shows the disease dynamics of all models. In Section 3, we observed that the SEIRb (and SEIR) models only exhibit disease free equilibria due to the lack of growth in the susceptible compartment, while the SEIRSb (and SEIRS) models have the capacity to reach an endemic equilibrium. Both the SEIR and SEIRS models reach their respective equilibrium very quickly, within about 200 days. However, for the endogenous models, the infectious population sizes are virtually indistinguishable initially, and the decay of the infectious population in the SEIRb model may take a very long time to occur (dependent on the size of the initial outbreak versus the size of the susceptible population). It may even look like an endemic equilibrium is reached (Fig. 2(b)). Given enough time, the disease does indeed die out (Fig. 2(c), nearly 400,000 days until apparent die out), as compared to the SEIRSb model, with its more biologically consistent inclusion of waning immunity, which allows for a true endemic equilibria. The appearance of an endemic equilibrium when there is not one is not necessarily contradictory to the behavior we observe in the current pandemic. Certainly, we see COVID-19 persisting but at a significantly reduced level from the first few years. It is possible that COVID-19 could die out over time, although this is unlikely given what we know about its features [52]. This does not reduce the usefulness of the SEIRb model as forecasting occurs within a relatively short window compared to disease dynamics; forecasting periods considered as long-term could fall within the time frame spanned by just one epidemic wave [4]. Nonetheless, a model which considers more characteristics of human behavior and disease dynamics produces more accurate results regarding disease behavior over time. For example, in Section 4.4, we also consider the addition of seasonality and observe how this further improves model validity.

4.2. Time-varying sensitivity analysis

We follow the methods from [7] to analyze the local sensitivity of model output with respect to base transmission rate, β; modified sensitivity to risk of infection, $a = \alpha N$; infection risk impact, γ; and period of immunity, τ_R.

We calculate sensitivity by the partial derivative of the solutions to the system with respect to the parameter of interest. For example, in the case of base transmission rate, β, we aim to determine

$$\frac{\partial s}{\partial \beta}, \ \frac{\partial e}{\partial \beta}, \ \frac{\partial i}{\partial \beta}, \ \frac{\partial r}{\partial \beta}, \ \frac{\partial f}{\partial \beta}.$$

We numerically approximate these partial derivatives by solving the system created by differentiating each of the previous partial derivatives with respect to t and also consider semi-relative sensitivity, which shows the partial derivatives scaled by the respective parameter, to allow for ease of comparison across parameters which differ in magnitude. We numerically solve the sensitivity systems (see Appendix C for equations) to obtain plots of the sensitivity of each solution with respect to parameters of interest (β, a, γ, τ_R), compared with the solution to the original systems and the semi-relative sensitivity in Fig. 3 (no behavior) and Fig. 4 (with behavior).

We can interpret the sensitivity plots by noting two characteristics: first, curve steepness in the sensitivity plots corresponds to changes in a solution's magnitude as the parameter values change, and (2) positivity (negativity) of partial derivatives in the sensitivity plots corresponds to solution magnitude increasing (decreasing) as the parameter values increase. For example, with the exogenous models (Fig. 3), the magnitude of solutions is increasing as β increases, up until about day 50. This corresponds to the initial positive portion of the sensitivity graphs. Then, between roughly days 50 and 80, the solutions begin to intersect, until the order is reversed around day 80. The magnitude of solutions now decreases as β increases, corresponding to the negative portion of the sensitivity graphs. For the SEIR model, the solutions do not intersect again before achieving the DFE (Fig. 3(d)), and the corresponding sensitivity graph changes from negative to zero (Figs. 3(b) and 3(c)). For the SEIRS model, the solutions oscillate and intersect again (Fig. 3(e)),

Table 4
Parameter values and ranges used in simulations and numerical sensitivity analyses. Any values used which differ from the values listed here are stated in the relevant figure captions.

Symbol	Initial conditions and parameters	Range	Value	Source
$s(0)$	Initial amount of susceptible individuals		$1-(2\times10^{-5})$	[a]
$e(0)$	Initial amount of exposed individuals		1×10^{-5}	[a]
$i(0)$	Initial amount of infectious individuals		1×10^{-5}	[a]
$r(0)$	Initial amount of recovered individuals		0	[a]
$f(0)$	Initial amount of perceived infections		0	[a]
β	Base transmission rate	$[0.1, 4]$	0.7	[4]
γ	(infection) risk diminishing impact	$[0, 5]$	2	[4]
α	Sensitivity to (risk of) infection	$[0, 100]$	1/30	[4]
N	Total population size	$[10^3, 10^8]$	10^6	[a]
a	Rescaled parameter, $a=\alpha N$	$[0, 10^{10}]$	$10^5/3$	[a]
τ_E	Exposure period	$[1, 5]$	5	[49]
τ_I	Infectious period	$[1, 14]$	10	[50]
τ_F	Time lag between infection awareness and infection occurrence	$[1, 200]$	20	[4]
τ_R	Period of immunity	$[1, 365]$	90	[51]

[a] Values chosen to represent initial outbreak size similar to those seen per 10^6 in the data (see Fig. 7).

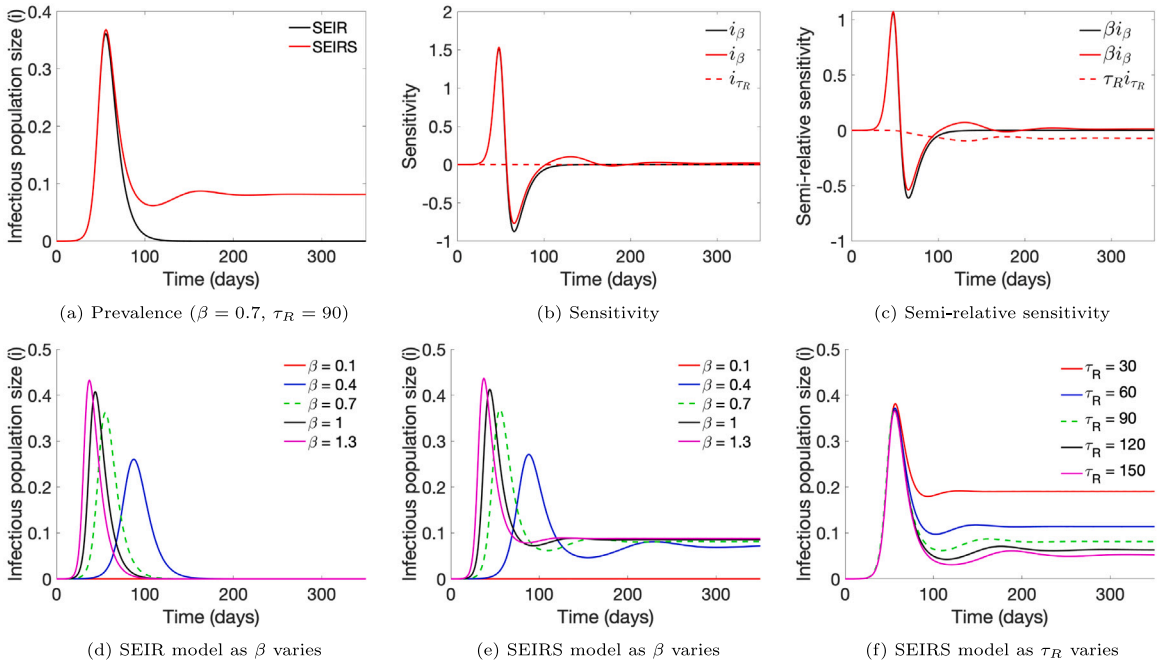

(a) Prevalence ($\beta = 0.7$, $\tau_R = 90$) (b) Sensitivity (c) Semi-relative sensitivity

(d) SEIR model as β varies (e) SEIRS model as β varies (f) SEIRS model as τ_R varies

Fig. 3. Sensitivity of SEIR and SEIRS models to changes in parameters. (a) Solutions to, (b) sensitivity of, and (c) semi-sensitivity of SEIR and SEIRS models. For (a)–(c), SEIR model in black and SEIRS model in red. Model solutions for differing values of (d) β (SEIR), (e) β (SEIRS), and (f) τ_R (SEIRS). For (d)–(f), standard parameter values are shown with a dashed line. For ease of visibility, we use the following notation to represent partial derivatives in (b) and (c): $x_y := \frac{\partial x}{\partial y}$.

resulting in continued sign changes in the sensitivity plots (Figs. 3(b) and 3(c)), before finally achieving the endemic equilibrium, which corresponds to the sensitivity plots reaching zero. While the SEIR and SEIRS model are sensitive to changes in β early in the infections (for roughly the first 100 and 200 days, respectively), the SEIRS model is not sensitive to changes in τ_R until roughly day 50 (after the outbreak peak is reached). Then, changes in τ_R primarily determine the size of the endemic equilibrium.

For the endogenous models, we use the plots displaying semi-relative sensitivity with respect to β as an example (Figs. 4(c) and 4(f)). Additionally, Fig. C.1 in Appendix C help illustrate the written interpretation of these results. The sensitivity curves for β initially display steep growth before hitting a maximum. As the steepness of this curve increases, the difference in magnitude of the solutions corresponding to different β values also increases. Once the sensitivity curves pass the first peak and begin to decrease, the difference in solutions decreases for differing β values. After the sensitivity curves pass the first trough and begin to increase again, the difference in solutions again increases for differing β values. This pattern continues as the sensitivity curves oscillate. As the oscillations dampen, there are smaller changes in the difference in solutions for differing β values; when oscillations cease, the solutions for differing β values remain a fixed distance apart. In addition, values that are negative (i.e. sensitivity with respect to γ and semi-relative sensitivity with respect to γ and a) represent an inverse relationship between parameter size and prevalence. For example, as a, the modified sensitivity to (risk of) infection, increases, infection numbers decrease.

Over the first 300 days, the SEIRb model is sensitive to changes in all three parameters, with a similar amount of sensitivity to β and γ (Fig. 4(c)). Although not as influential as the other two, a also influences model dynamics. We repeat our time-varying sensitivity analysis with the SEIRSb model and find nearly identical results for β, γ and a, and essentially no sensitivity to changes in the additional parameter τ_R (Figs. 4(e), 4(f)). This is expected as the loss of immunity occurs much slower than behavioral response, and does not dominate over the course of 350 days, the time-frame considered in Fig. 4.

One key difference between the exogenous and endogenous models with waning immunity is the sensitivity to τ_R, the period of immunity.

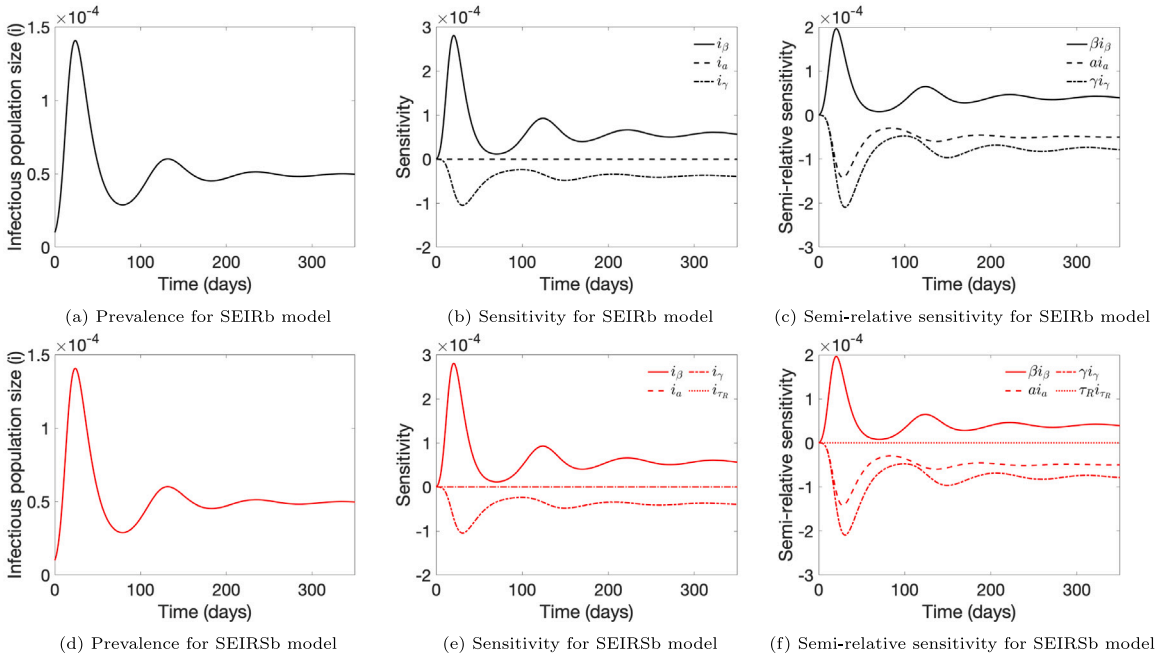

(a) Prevalence for SEIRb model (b) Sensitivity for SEIRb model (c) Semi-relative sensitivity for SEIRb model

(d) Prevalence for SEIRSb model (e) Sensitivity for SEIRSb model (f) Semi-relative sensitivity for SEIRSb model

Fig. 4. Sensitivity of SEIRb and SEIRSb models to changes in parameters. (a) Solution to, (b) sensitivity of, and (c) semi-sensitivity of SEIRb model (black). (d) Solution to, (e) sensitivity of, and (f) semi-sensitivity of SEIRSb model (red). (a)–(c), the SEIR model, are essentially identical to (d)–(f), the SEIRSb model. The corresponding solutions for changes in parameters,as in Fig. 3(d)–(f), are found in Appendix C. Note that i_{τ_R} and i_a are overlapping in Figure 4(e).

The SEIRS model shows slight sensitivity to τ_R (although primarily when the outbreak reaches the endemic equilibrium), but the SEIRSb model does not show any effect from changes to the period of immunity, indicating that the inclusion of behavior overrides influences of waning immunity in the model, at least across one year. With respect to disease control, changes to the period of immunity would not significantly alter initial outbreak dynamics, and with the inclusion of human behavior, any impacts would not be apparent on the time scale of a single wave.

Another difference between the exogenous and endogenous models (regardless of the immunity mechanism considered) is in sensitivity with respect to β. With the exogenous models, β substantially controls solution magnitude, peak timing, and peak widths, and has a minor impact on the endemic equilibrium. As β changes, all of these change as well. However, in the endogenous models, only solution magnitude and the endemic equilibrium change as β changes; peak timing and width remain relatively the same (Fig. C.1 in Appendix C). Once again, the inclusion of behavior is sufficient to override these specific influences of β on the model. This indicates that controlling base transmission rate, when considering the effects of human behavior, will only serve to change outbreak magnitude and will not affect the timing of the outbreak peak or flatten the curve.

The most influential parameters on disease dynamics for both endogenous models are the transmission rate β and the infection risk diminishing impact, γ, and both endogenous models show the most sensitivity to these parameters early in an outbreak. Thus, mitigation strategies that reduce the base transmission rate or diminish the impact of infection risk can aid in controlling the magnitude and speed of an outbreak. This is consistent with intuition of outbreak control: decreasing transmission and increasing the impact of the risk of infection can slow the spread of the disease. This reinforces the need for continued focus on these by policy makers to mitigate the impact of an outbreak.

4.3. Global sensitivity analysis

We next perform global sensitivity analysis via Latin Hypercube Sampling with Partial Rank Correlation Coefficients (LHS/PRCC) [53] to obtain results on which parameters have stronger influence on model outputs. We use the same sampling of 10,000 parameter sets for all models, chosen uniformly from the ranges indicated in Table 4 and use the `partialcorr` function in MATLAB, using a Spearman coefficient, to calculate PRCC. Prior to finding the PRCC, we confirm the monotonicity of relationships between the parameters and respective quantities of interest (not shown). Note that parameter a from the rescaled models depends on both α and N, so we consider the latter two parameters separately in this sensitivity analysis, noting that we can obtain results for a through the relationships $a = \alpha N$. We consider three specific quantities of interest (QOIs) to give a picture of disease dynamics over time: (1) maximum size of the infectious population; (2) infectious population size at 50 days; (3) infectious population size at 2 years. To aid in interpretation of the results, it is helpful to note that a positive (negative) PRCC indicates a positive (negative) correlation between change in parameter size and QOI magnitude, when controlling for linear effects of other parameters [53]. Larger PRCC values indicate stronger impacts of parameter change on QOI magnitude, and a p-value > 0.05 is not considered significant. In Fig. 5, all parameters have significant p-values, with the exception of τ_R in the SEIRSb model (all QOI) and τ_E in the SEIRS model (QOI 3).

As with the time-varying sensitivity analysis, we see very similar results for parameter influence between models with waning immunity and models which exclude waning immunity, i.e. between the SEIR and SEIRS models, and between the SEIRb and SEIRSb models. Only the models with waning immunity (SEIRS and SEIRSb models) include the parameter τ_R, which measures the period of waning immunity.

We first focus on the exogenous model comparisons (Fig. 5, left column). For the maximum size of the infectious population (QOI 1), each parameter has essentially the same PRCC value for both the SEIR and SEIRS models. For all three QOIs, τ_I has the largest positive impact and is the most influential parameter for QOIs 1 and 2. For the infectious population size at 2 years (QOI 3), τ_I and τ_E are close in magnitude, although opposite in sign, for the SEIR model. The impact of τ_E diminishes with each successive QOI, and loses significance for the SEIRS model at two years (QOI 3). Base transmission rate, β, has a large positively correlated impact on the peak size of an outbreak (QOI 1), but for infectious population at 50 days (QOI 2), β has a negative impact, supported by observations from Figs. 3(d) and 3(e).

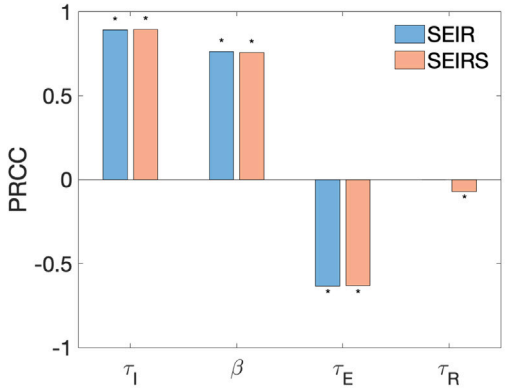

(a) QOI 1: maximum size of the infectious population

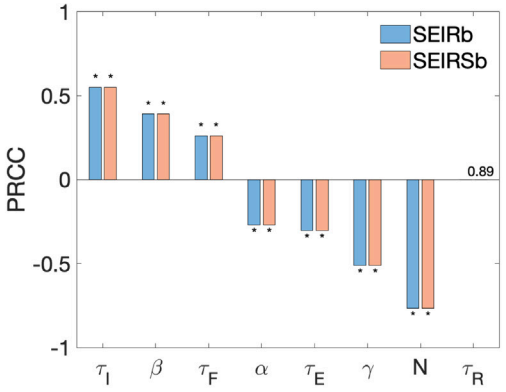

(b) QOI 1: maximum size of the infectious population

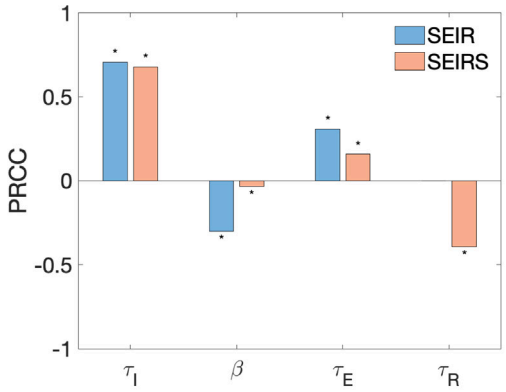

(c) QOI 2: infectious population at 50 days

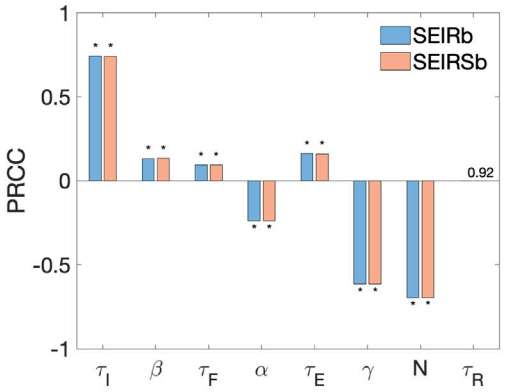

(d) QOI 2: infectious population at 50 days

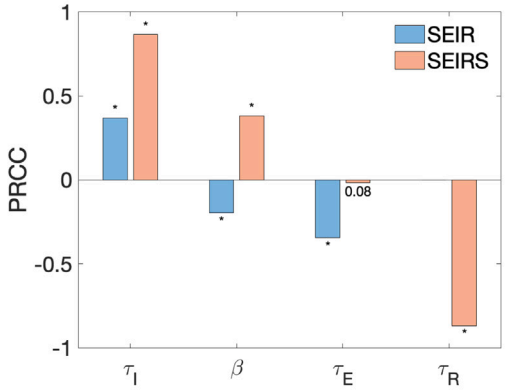

(e) QOI 3: infectious population size at 2 years

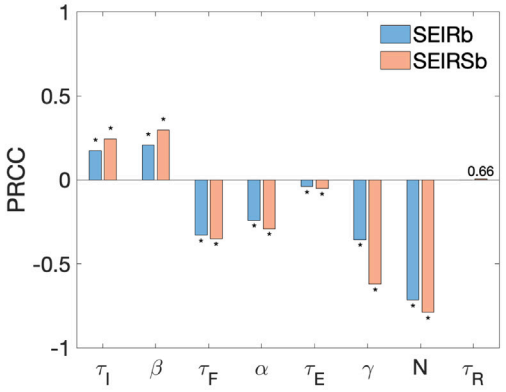

(f) QOI 3: infectious population size at 2 years

Fig. 5. Global sensitivity analysis for all models with three different quantities of interest (QOI). Left column shows SEIR/SEIRS model results; right column shows SEIRb/SEIRSb model results. QOIs are: maximum size of infectious population (a)–(b); infectious population at 50 days (c)–(d); and infectious population at 2 years (e)–(f), when most parameter sets have reached a (quasi-) equilibrium. *p*-values are given above/below each respective bar. *indicates *p*-values below 0.001.

For the SEIRS model, as the time point of model output progresses (QOI 1 to QOI 2 to QOI 3), the impact of τ_R increases. This agrees with observations from Fig. 3(f) which only shows change in solution magnitude around the endemic equilibrium as τ_R changes.

The infectious population at two years (QOI 3) gives an indication of how parameters affect the approach to the disease free equilibria (SEIR) and endemic equilibrium (SEIRS). All four parameters for the SEIRS model have strong impact on the value of the endemic equilibrium, supported by observations from Figs. 3(e) and 3(f) and the closed form solution of the endemic equilibrium found in Appendix A. Interestingly, for the SEIR model, the three parameters appear to affect the magnitude of the disease free equilibrium (approximated by QOI 3), an apparent contradiction since i should be, by definition, approach zero. This is due to the fact that the solution never truly reaches zero in finite time. The approach to zero (as measured at two years in QOI 3) is impacted by the parameters. When we assume that very small infectious populations ($< 10^{-10}$) can be considered to be zero and examine a later time point, there is no significant impact of any of the three parameters on the disease free equilibrium of the SEIR model, as expected.

Next, we examine the endogenous SEIRb and SEIRSb model results (Fig. 5, right column). For QOIs 1 and 2, these models display essentially the same PRCC values for nearly all parameters (Note that τ_R only appears in the SEIRSb model and is never significant). However, for the infectious population at two years (QOI 3), we observe differing results as each model begins to approach its respective equilibrium (disease free equilibria for the SEIRb and endemic equilibrium for the SEIRSb).

Additionally, the most influential parameters (τ_I β, γ, and N) remain the same for each QOI, although for QOI 3, the order of τ_I and β is reversed and τ_F has a similar impact in magnitude to τ_I, β, and γ. The parameters N and α show roughly the same negative influence for each QOI, with α showing about 50% of effect of N.

Interestingly, τ_E is negative for QOI 1, positive for QOI 2, and rather small (albeit still statistically significant) for QOI 3, supported by dynamics in Fig. C.1. This is because increases in the latent period, τ_E, increase initial peak height and shorten the timing to the initial peak (positive correlations for QOI 1), but the ordering reverses by 50 days (QOI 2) because earlier and larger peaks decline more quickly. Additionally, increases in the lag between infection and response, τ_F, also flip the direction of influence from QOI 1 and 2 (positive) to QOI 3 (negative) and has the strongest, but negative, influence on QOI 3. Larger τ_F, indicating longer delay between infection occurrence and response, lengthens the periods between oscillations, which lengthens the time until oscillations damp out (Fig. C.1).

When comparing the models without the endogenous behavior component (SEIR and SEIRS) to the models with the endogenous behavior component (SEIRb and SEIRSb), we observe key differences in all three QOIs. For maximum infectious peak (QOI 1), all parameters have a stronger affect on the exogenous models, but impact all four models the same with respect to direction (positive and negative correlations). For the infectious population size at 50 days (QOI 2), the exogenous models begin to differ in sensitivity (SEIR vs. SEIRS), whereas the endogenous models show the same sensitivity to all parameters (SEIRb vs. SEIRSb). Furthermore, the base transmission rate β exhibits negative PRCC for the exogenous models but positive PRCC for the endogenous models, as peak timing changes with β in the exogenous models but not in the endogenous ones. For infectious population size at two years (QOI 3), the infectious period, τ_I, remains more significant than β in the exogenous models, but the reverse holds for the endogenous models. The effect of τ_E is small in QOI 3 for all models. Finally, τ_R has a much stronger impact on all QOIs for the exogenous models, while it never has a significant impact on endogenous models.

This global sensitivity analysis supports several results from the time-varying sensitivity analysis. First, τ_R has virtually no influence on endogenous SEIRSb model dynamics but strongly impacts the dynamics at later time points for the SEIRS model. However, as τ_R impacts the endemic equilibrium of both SEIRS and SEIRSb models, the additional assumption of waning immunity, which better reflects reality, provides richer equilibria dynamics for both models. Biologically, the impact of waning immunity is minimal in the short time frame of two years considered in this sensitivity analysis, especially when considering behavior. Despite this, it has the potential to show more long-term affects in the endogenous models that what is explored here. Second, base transmission rate, β, and infection risk diminishing impact, γ, strongly influence disease dynamics, but sensitivity to risk of infection, α, only has a small impact. Note that in the time-varying sensitivity analysis, α's impact is inflated by multiplication by N. The global sensitivity analysis also indicates that duration of infectiousness, τ_I, has a very strong effect on outbreak size. Thus, reducing infectiousness, e.g. through masking and self-quarantine, is highly instrumental in decreasing the number of infections that occur throughout the timeline of the disease. Lastly, focusing on keeping awareness of infection risk high (i.e. maintaining large γ values) will greatly aid in reduction of infections.

4.4. Model validation with COVID-19 data

We demonstrate each model's fidelity in replicating COVID-19 data across each state of the United States, as well as the District of Columbia (totaling 51 US regions). The inclusion of a large number of regions ensures rigorous testing against various pandemic patterns, considering regions with different populations, behavioral responses, and potentially differing regional government policies. Our testing is limited to the period up to May 1st, 2021. We chose this endpoint to exclude the effects of vaccinations, which predominantly became available during and after the summer of 2021, as well as the Delta and Omicron variants, which exhibited different infectivity and fatality rates. Using a data range spanning over one year allows us to go beyond a single wave and test the model's ability to recreate multiple waves of the pandemic endogenously. We focus on replicating death data (seven-day rolling average) as it is more accurately reported than the COVID-19 case data.

Table 5
Model performance (R-squared) in replicating summary US data.

	SEIRS	SEIRS with seasonality	SEIRSb	SEIRb with seasonality	SEIRSb with seasonality
Regional average	0.19	0.19	0.65	0.78	0.79
Regional median	0.02	0.02	0.70	0.83	0.84
Combined USA	0.04	0.42	0.93	0.94	0.95

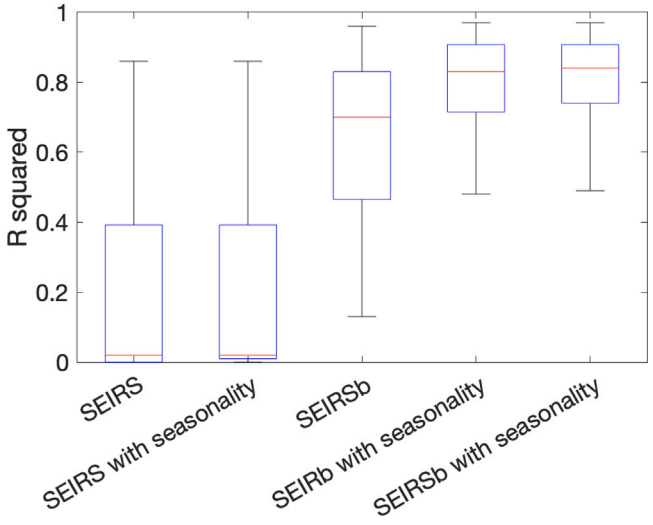

Fig. 6. Distribution of R-squared of 5 different models across 51 US regions. Red line is the median, blue box is 25%–75% percentile, and whiskers represent the 95% interval.

We tested both the rescaled SEIRb and SEIRSb models (Systems (2) and (4), respectively) and compared their performance against base models of SEIR or SEIRS that exclude the behavioral feedback loop. To account for changes in infectivity due to seasonality, we also incorporated a simple sinusoidal seasonality pattern into infectivity with a period of 365 days (See Appendix D for details). Given that government policies are implemented in response to changes in risk levels, the behavioral feedback loop represents the aggregate societal response (government and people). Thus, we did not need to include government inputs to the model but rather have the model replicate the overall societal response endogenously. To estimate the unknown parameters, we minimized the mean square errors between simulation and daily death data (per capita) for each state. In the model, we calculate daily per capita death, d, as

$$d = IFR\left(\frac{i}{\tau_I}\right), \tag{11}$$

where IFR is the infection fatality rate, which we assume is 0.5% [54]. The parameters that were fitted and the range of values assumed during the model calibration process are reported in Appendix D and listed in Table D.1.

The best-performing model is the SEIRSb model with a simple seasonality effect. Overall, our analysis indicates that the model exhibits excellent performance in replicating most of the states of the US with average and median R-squared values across US regions of 0.79 and 0.84, respectively (Table 5 and Fig. 6). To demonstrate how each model fits to the data, Fig. D.2 shows fits for all models to the combined US

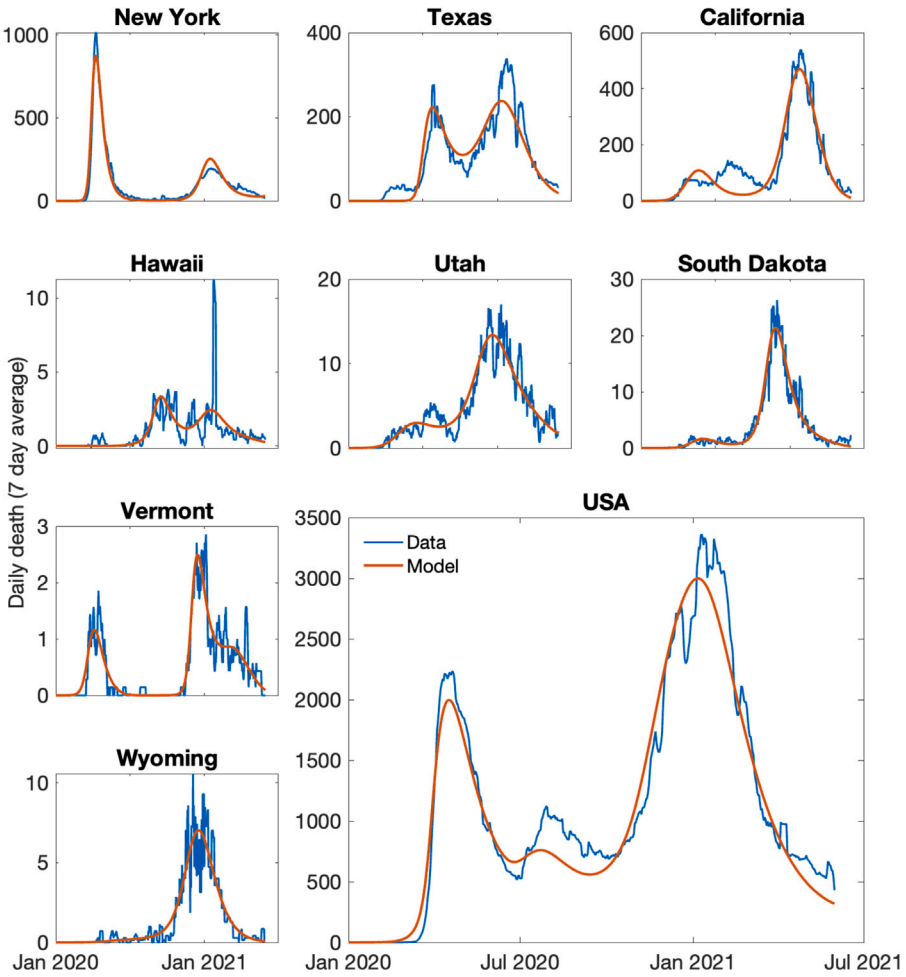

Fig. 7. A sample of replication of COVID-19 daily death (seven day rolling average) across US regions and the US selected to show a range of performance in replicating varying modes of outcomes. Blue lines are reported death data (per capita), and red lines are model death data (per capita). See Appendix Fig. D.3 for all US regions.

data. The R-squared results for each of the 51 regions are reported in Appendix D, Table D.2. Results from a sample of 8 regions and the overall United States daily deaths are presented in Fig. 7. The regions shown were selected to include a range of regions with varying populations, shapes of graphs, and model performance. Specifically, in this sample of 8 states, the model performs very well in replicating the states of New York and South Dakota, even though they have different patterns and populations. The model's performance in high-population states such as California and Texas is reasonable even though we note that a relatively small wave is missed in both cases. The performance of the model in the lower population states of Vermont and Wyoming is also very good. A few states, such as Hawaii, had corrections to their data (note the large spike in early 2021) which resulted in a few outliers in their reports, thus bringing down the R-squared. We intentionally did not change the reported raw data of states. Adding all 50 states and the District of Columbia closely replicates US data (R-squared of 0.95). The graphs for all regions are available in Appendix D, Fig. D.3.

The results from the SEIRb model – that does not include waning immunity – are only slightly weaker that SEIRSb, holding an average R-squared of 0.78. Both SEIRSb and SEIRb models outperform the base model that excludes behavioral feedback considerably in R-squared (Fig. 6). The results from all tested models for each region in the United States, as well as additional details on the model fitting are reported in Appendix D.

Overall, these tests underscore two key points: (1) the model's capability to replicate pandemic data across a large sample of regions and over multiple waves of a pandemic, and (2) the significance of the behavioral feedback loop in improving the fit between simulation and data.

5. Conclusions

In this work, we consider two influences on COVID-19 spread which can strengthen epidemic models: endogenous incorporation of human behavior and the addition of waning immunity. We analyze, simulate, and validate simple epidemic models, both exogenous and endogenous, with permanent immunity (SEIR and SEIRb) and with waning immunity (SEIRS and SEIRSb). The core mechanism in both endogenous models is a negative feedback loop that represents change in societal risk response over the course of a pandemic: as the disease prevalence increases, perceived risk increases leading to compliance with public health measures that lowers new cases and prevalence. This feedback loop leads to the cycles of compliance and complacency, creating oscillatory patterns in prevalence.

The inclusion of human behavior through such a feedback loop strongly affects model dynamics, as shown in our sensitivity analysis. While exogenous model dynamics are sensitive to changes in parameters base transmission rate, β, and waning immunity period, τ_R, with the inclusion of behavior (through the addition of parameters: sensitivity to risk of infection, a, risk diminishing impact, γ, and time lag between occurrence of and response to infection, τ_F), endogenous models exhibit less sensitivity to changes in β and virtually no sensitivity to changes in τ_R. Additionally, the endogenous incorporation of behavior allows these simple models (SEIRb and SEIRSb) to provide

better fits and ability to forecast than models that do not explicitly include human behavior or do so exogenously.

With the inclusion of behavior, distinctions are much more subtle between the permanent immunity and waning immunity models in numerical simulations, sensitivity analysis, and identifiability analysis. Differences between these endogenous models appear when considering long-term dynamics, due to the existence of an endemic equilibrium in the SEIRSb (SEIRS) model which is not present in the SEIRb (SEIR) model. Other than providing the existence of an endemic equilibrium, waning immunity does not strongly influence short-term model dynamics. Indeed, sensitivity analyses show that τ_R has essentially no impact on the SEIRSb model over the first two years. Model validation shows that the SEIRSb model gives only slightly more realistic predictions and has a marginally better fit to the COVID-19 data than the SEIRb model. However, given that it provides the existence of an endemic equilibrium, with little to no trade off in model complexity, indicates that the inclusion of waning immunity is valuable when formulating models for long-term forecasting, but may not be necessary for short-term parameter estimation.

Models with similar endogenous transmission mechanisms to the SEIRb and SEIRSb models exist [27,28,55], many of which are categorized in the review [32]. While these models can be classified according to the mechanism used to represent human behavior, the assumptions surrounding other aspects of model structure can result in different outcomes between models which have the same type of behavior mechanism. For example, Weitz et al. [28] use a similar fractional formulation of transmission to the SEIRb model; however, transmission is formulated as a function of deaths rather than prevalence. They also include a time lag between infections and fatalities, similar to the time lag included in the SEIRb model (see Section 2). However, these formulations result in differing disease dynamics: in [28], outbreak peaks are asymmetric, with a sharp increase to the peak followed by a slow decline while the SEIRb model retains more symmetry within outbreak waves. Weitz et al. additionally include adherence fatigue and long-term behavior change to adjust the model to show consistent results with data with respect to pre-peak increases in mobility. These additions to model structure go beyond those behavior considerations incorporated in the SEIRb model. This leads to a key question addressed throughout this work: what level of complexity needs to be considered in model structure to result in good model fit to data? Section 4.4 discusses this through the addition of human behavior, seasonality, and disease death when fitting to data.

Future studies can benefit from expanding risk response mechanisms in several ways. These include incorporating different demographics and age structures, considering other behavioral feedback loops such as the willingness to vaccinate, health policy compliance, and adherence fatigue, as well as conducting statistical examinations of factors that affect human behavior. Additionally, understanding how these factors impact the spread of the disease can provide valuable insights.

In conclusion, incorporation of human behavior into epidemic models provides for more realistic feedback loops that react on the time scale of infection dynamics. Thus, when using models to inform policy, endogenous incorporation of human behavior is highly recommended, but inclusion of waning immunity can depend upon the relevant time period being considered.

CRediT authorship contribution statement

Leah LeJeune: Writing – review & editing, Writing – original draft, Visualization, Validation, Software, Methodology, Investigation, Formal analysis, Data curation, Conceptualization. **Navid Ghaffarzadegan:** Writing – review & editing, Writing – original draft, Visualization, Validation, Supervision, Project administration, Methodology, Investigation, Funding acquisition, Data curation, Conceptualization. **Lauren M. Childs:** Writing – review & editing, Writing – original draft, Visualization, Validation, Supervision, Project administration, Methodology, Investigation, Funding acquisition, Formal analysis, Conceptualization. **Omar Saucedo:** Writing – review & editing, Writing – original draft, Visualization, Validation, Supervision, Project administration, Methodology, Investigation, Funding acquisition, Formal analysis, Conceptualization.

Declaration of competing interest

None

Data availability

Source code and simulated data will be made publicly available on GitHub upon acceptance. Source code and simulated data are available by request during review.

Acknowledgments

This work was supported by the US National Science Foundation, Division of Mathematical Sciences, USA and Division of Social and Economic Sciences, USA , Award # 2229819.

Appendix A. Equations and equilibria for exogenous models: SEIR and SEIRS

The SEIR and SEIRS models without behavioral feedback are similar to Eqs. (2) and (4), respectively, except that the transmission term is constant rather than a function of F, i.e., $\beta(F) = \beta$. Thus, there is no need for an equation for perceived infectious, f

With permanent immunity, the normalized SEIR model is given by

$$\begin{aligned} \frac{ds}{dt} &= -\beta si, \\ \frac{de}{dt} &= \beta si - \frac{e}{\tau_E}, \\ \frac{di}{dt} &= \frac{e}{\tau_E} - \frac{i}{\tau_I}, \\ \frac{dr}{dt} &= \frac{i}{\tau_I}. \end{aligned} \tag{A.1}$$

With waning immunity, the normalized SEIRS model is given by

$$\begin{aligned} \frac{ds}{dt} &= -\beta si + \frac{r}{\tau_R}, \\ \frac{de}{dt} &= \beta si - \frac{e}{\tau_E}, \\ \frac{di}{dt} &= \frac{e}{\tau_E} - \frac{i}{\tau_I}, \\ \frac{dr}{dt} &= \frac{i}{\tau_I} - \frac{r}{\tau_R}. \end{aligned} \tag{A.2}$$

We summarize the equilibria and their existence and stability in Table A.1, which have been previously described in other contexts [7]. The basic reproductive number, $\mathcal{R}_0 = \beta\tau_I$, is identical for the SEIR, SEIRS, SEIRb and SEIRSb models.

Appendix B. Identifiability of exogenous models: SEIR and SEIRS

The SEIR and SEIRS models with all initial conditions for state variables known and unknown parameters are globally identifiable (Theorem B.1 and Theorem B.3, respectively). When the initial conditions for the state variables and model parameters are unknown, the SEIR and SEIRS models are locally identifiable (Theorem B.2 and Theorem B.4, respectively).

Theorem B.1. *Identifiability of SEIR model with known initial conditions.*

The SEIR model given by System (A.1) is globally identifiable when all initial conditions for the state variables are known and prevalence (size of class i) is the output measure.

Table A.1
Equilibria for SEIR model and SEIRS model assuming biologically relevant parameters, i.e., $\{\beta, a, \gamma, \tau_E, \tau_I, \tau_F, \tau_R\} > 0$, and biologically realistic initial conditions, i.e., $\{s(0), e(0), i(0), r(0)\} \in [0, 1]$.

Model	Equilibrium type	Values	Existence, uniqueness, and stability
SEIR	Disease free (DFE)	$(\bar{s}, 0, 0, \bar{r}, 0),\ \bar{s} + \bar{r} = 1$	There always exists a line of DFE.
SEIRS	Disease free (DFE)	$(1, 0, 0, 0, 0)$	Always exists and is a unique DFE Locally asymptotically stable when $\mathcal{R}_0 < 1$ Unstable when $\mathcal{R}_0 > 1$
	Endemic (EE)	$\left(\frac{1}{\mathcal{R}_0}, \frac{\tau_E}{\tau_I}\bar{i}, \bar{i}, \frac{\tau_R}{\tau_I}\bar{i}\right),\ \bar{i} = \frac{(\mathcal{R}_0 - 1)\tau_I}{\mathcal{R}_0(\tau_E + \tau_I + \tau_R)}$	Exists and is a unique stable EE when $\mathcal{R}_0 > 1$ Does not exist when $\mathcal{R}_0 \leq 1$

Proof. Let $\mathbf{p}_1 = \{\beta, \tau_I, \tau_E\}$ and $\mathbf{p}_2 = \{\hat{\beta}, \hat{\tau_I}, \hat{\tau_E}\}$. Suppose that $y(t, \mathbf{p_1}) = y(t, \mathbf{p_2})$. Then we obtain the following functional relationships from *StructuralIdentifiability.jl*:

$$\beta = \hat{\beta}, \quad \tau_E = \hat{\tau}_E, \quad \tau_I = \hat{\tau}_I. \tag{B.1}$$

Thus, $\mathbf{p}_1 = \mathbf{p}_2$ which entails that the SEIR model is globally structurally identifiable with respect to prevalence data. □

Theorem B.2. *Identifiability of SEIR model with unknown initial conditions.*

The SEIR model given by System (A.1) is locally identifiable when all initial conditions for the state variables are unknown and prevalence (size of class i) is the output measure.

Proof. Let $\mathbf{p}_1 = \{\beta, \tau_I, \tau_E\}$ and $\mathbf{p}_2 = \{\hat{\beta}, \hat{\tau_I}, \hat{\tau_E}\}$. Suppose that $y(t, \mathbf{p_1}) = y(t, \mathbf{p_2})$. Then we obtain the following functional relationships from *StructuralIdentifiability.jl*:

$$\beta = \hat{\beta}, \quad \tau_E\tau_I = \hat{\tau}_E\hat{\tau}_I, \quad \tau_E + \tau_I = \hat{\tau}_E + \hat{\tau}_I. \tag{B.2}$$

Solving the System (B.2) using *Mathematica*, we generate two set of solutions:

$$\begin{aligned}&\{\beta = \hat{\beta},\ \tau_I = \hat{\tau}_E,\ \tau_E = \hat{\tau}_I\},\\ &\{\beta = \hat{\beta},\ \tau_I = \hat{\tau}_I,\ \tau_E = \hat{\tau}_E\}.\end{aligned} \tag{B.3}$$

This means that the SEIR model is locally identifiable with respect to prevalence data. □

Theorem B.3. *Identifiability of SEIRS model with known initial conditions.*

The SEIRS model given by System (A.1) is globally identifiable when all initial conditions for the state variables are known and prevalence (size of class i) is the output measure.

Proof. Let $\mathbf{p}_1 = \{\beta, \tau_I, \tau_E, \tau_R\}$ and $\mathbf{p}_2 = \{\hat{\beta}, \hat{\tau_I}, \hat{\tau_E}, \hat{\tau}_R\}$. Suppose that $y(t, \mathbf{p_1}) = y(t, \mathbf{p_2})$. Then we obtain the following functional relationships from *StructuralIdentifiability.jl*:

$$\beta = \hat{\beta}, \quad \tau_E = \hat{\tau}_E, \quad \tau_I = \hat{\tau}_I, \quad \tau_R = \hat{\tau}_R. \tag{B.4}$$

Thus, $\mathbf{p}_1 = \mathbf{p}_2$ which entails that the SEIRS model is globally structurally identifiable with respect to prevalence data. □

Theorem B.4. *Identifiability of SEIRS model with unknown initial conditions.*

The SEIRS model given by System (A.2) is locally identifiable when all initial conditions for the state variables are unknown and prevalence (size of class i) is the output measure.

Proof. Let $\mathbf{p}_1 = \{\beta, \tau_I, \tau_E, \tau_R\}$ and $\mathbf{p}_2 = \{\hat{\beta}, \hat{\tau_I}, \hat{\tau_E}, \hat{\tau_R}\}$. Suppose that $y(t, \mathbf{p_1}) = y(t, \mathbf{p_2})$. Then we obtain the following functional relationships from *StructuralIdentifiability.jl*:

$$\beta = \hat{\beta}, \quad \tau_E\tau_I = \hat{\tau}_E\hat{\tau}_I, \quad \tau_E + \tau_I = \hat{\tau}_E + \hat{\tau}_I, \quad \tau_R = \hat{\tau}_R. \tag{B.5}$$

Solving the System (B.5) using *Mathematica*, we generate two set of solutions:

$$\{\beta = \hat{\beta},\ \tau_I = \hat{\tau}_E,\ \tau_E = \hat{\tau}_I, \tau_R = \hat{\tau}_R\},$$

$$\{\beta = \hat{\beta},\ \tau_I = \hat{\tau}_I,\ \tau_E = \hat{\tau}_E, \tau_R = \hat{\tau}_R\}. \tag{B.6}$$

This means that the SEIRS model is locally identifiable with respect to prevalence data. □

Appendix C. Time-varying sensitivity equations and reference plots

Here, we include the time-varying sensitivity equations used in the simulation of Figs. 3 and 4.

C.1. Permanent immunity, exogenous: SEIR

Sensitivity equations with respect to β:

$$\begin{aligned}\frac{d}{dt}\left(\frac{\partial s}{\partial \beta}\right) &= \frac{\partial \dot{s}}{\partial \beta} + \frac{\partial \dot{s}}{\partial s}\frac{\partial s}{\partial \beta} + \frac{\partial \dot{s}}{\partial e}\frac{\partial e}{\partial \beta} + \frac{\partial \dot{s}}{\partial i}\frac{\partial i}{\partial \beta} + \frac{\partial \dot{s}}{\partial r}\frac{\partial r}{\partial \beta},\\ &= -si - \beta i\frac{\partial s}{\partial \beta} - \beta s\frac{\partial i}{\partial \beta},\\ \frac{d}{dt}\left(\frac{\partial e}{\partial \beta}\right) &= si + \beta i\frac{\partial s}{\partial \beta} - \frac{1}{\tau_E}\frac{\partial e}{\partial \beta} + \beta s\frac{\partial i}{\partial \beta},\\ \frac{d}{dt}\left(\frac{\partial i}{\partial \beta}\right) &= \frac{1}{\tau_E}\frac{\partial e}{\partial \beta} - \frac{1}{\tau_I}\frac{\partial i}{\partial \beta},\\ \frac{d}{dt}\left(\frac{\partial r}{\partial \beta}\right) &= \frac{1}{\tau_I}\frac{\partial i}{\partial \beta}.\end{aligned}$$

C.2. Waning immunity, exogenous: SEIRS

Sensitivity equations with respect to β:

$$\begin{aligned}\frac{d}{dt}\left(\frac{\partial s}{\partial \beta}\right) &= -si - \beta i\frac{\partial s}{\partial \beta} - \beta s\frac{\partial i}{\partial \beta} + \frac{1}{\tau_r}\frac{\partial r}{\partial \beta},\\ \frac{d}{dt}\left(\frac{\partial e}{\partial \beta}\right) &= si + \beta i\frac{\partial s}{\partial \beta} - \frac{1}{\tau_E}\frac{\partial e}{\partial \beta} + \beta s\frac{\partial i}{\partial \beta},\\ \frac{d}{dt}\left(\frac{\partial i}{\partial \beta}\right) &= \frac{1}{\tau_E}\frac{\partial e}{\partial \beta} - \frac{1}{\tau_I}\frac{\partial i}{\partial \beta},\\ \frac{d}{dt}\left(\frac{\partial r}{\partial \beta}\right) &= \frac{1}{\tau_I}\frac{\partial i}{\partial \beta} - \frac{1}{\tau_r}\frac{\partial r}{\partial \beta}.\end{aligned}$$

Sensitivity equations with respect to τ_R:

$$\begin{aligned}\frac{d}{dt}\left(\frac{\partial s}{\partial \tau_R}\right) &= -\frac{r}{\tau_R^2} - \beta i\frac{\partial s}{\partial \tau_R} - \beta s\frac{\partial i}{\partial \tau_R} + \frac{1}{\tau_R}\frac{\partial r}{\partial \tau_R},\\ \frac{d}{dt}\left(\frac{\partial e}{\partial \tau_R}\right) &= \beta i\frac{\partial s}{\partial \tau_R} - \frac{1}{\tau_E}\frac{\partial e}{\partial \tau_R} + \beta s\frac{\partial i}{\partial \tau_R},\\ \frac{d}{dt}\left(\frac{\partial i}{\partial \tau_R}\right) &= \frac{1}{\tau_E}\frac{\partial e}{\partial \tau_R} - \frac{1}{\tau_I}\frac{\partial i}{\partial \tau_R},\\ \frac{d}{dt}\left(\frac{\partial r}{\partial \tau_R}\right) &= \frac{r}{\tau_R^2} + \frac{1}{\tau_I}\frac{\partial i}{\partial \tau_R} - \frac{1}{\tau_R}\frac{\partial r}{\partial \tau_R}.\end{aligned}$$

C.3. Permanent immunity, endogenous: SEIRb

Sensitivity equations with respect to β:

$$\begin{aligned}
\frac{d}{dt}\left(\frac{\partial s}{\partial \beta}\right) &= -\frac{1}{(1+af)^{\gamma}} si - \frac{\beta}{(1+af)^{\gamma}} i\frac{\partial s}{\partial \beta} - \frac{\beta}{(1+af)^{\gamma}} s\frac{\partial i}{\partial \beta} \\
&\quad + \frac{a\beta\gamma}{(1+af)^{\gamma+1}} si\frac{\partial f}{\partial \beta}, \\
\frac{d}{dt}\left(\frac{\partial e}{\partial \beta}\right) &= \frac{1}{(1+af)^{\gamma}} si + \frac{\beta}{(1+af)^{\gamma}} i\frac{\partial s}{\partial \beta} - \frac{1}{\tau_E}\frac{\partial e}{\partial \beta} \\
&\quad + \frac{\beta}{(1+af)^{\gamma}} s\frac{\partial i}{\partial \beta} - \frac{a\beta\gamma}{(1+af)^{\gamma+1}} si\frac{\partial f}{\partial \beta}, \\
\frac{d}{dt}\left(\frac{\partial i}{\partial \beta}\right) &= \frac{1}{\tau_E}\frac{\partial e}{\partial \beta} - \frac{1}{\tau_I}\frac{\partial i}{\partial \beta}, \\
\frac{d}{dt}\left(\frac{\partial r}{\partial \beta}\right) &= \frac{1}{\tau_I}\frac{\partial i}{\partial \beta}, \\
\frac{d}{dt}\left(\frac{\partial f}{\partial \beta}\right) &= \frac{1}{\tau_F}\left(\frac{\partial i}{\partial \beta} - \frac{\partial f}{\partial \beta}\right).
\end{aligned}$$

Sensitivity equations with respect to a:

$$\begin{aligned}
\frac{d}{dt}\left(\frac{\partial s}{\partial a}\right) &= \frac{\beta\gamma f}{(1+af)^{\gamma+1}} si - \frac{\beta}{(1+af)^{\gamma}} i\frac{\partial s}{\partial a} - \frac{\beta}{(1+af)^{\gamma}} s\frac{\partial i}{\partial a} \\
&\quad + \frac{a\beta\gamma}{(1+af)^{\gamma+1}} si\frac{\partial f}{\partial a}, \\
\frac{d}{dt}\left(\frac{\partial e}{\partial a}\right) &= -\frac{\beta\gamma f}{(1+af)^{\gamma+1}} si + \frac{\beta}{(1+af)^{\gamma}} i\frac{\partial s}{\partial a} - \frac{1}{\tau_E}\frac{\partial e}{\partial a} \\
&\quad + \frac{\beta}{(1+af)^{\gamma}} s\frac{\partial i}{\partial a} - \frac{a\beta\gamma}{(1+af)^{\gamma+1}} si\frac{\partial f}{\partial a}, \\
\frac{d}{dt}\left(\frac{\partial i}{\partial a}\right) &= \frac{1}{\tau_E}\frac{\partial e}{\partial a} - \frac{I}{\tau_I}\frac{\partial i}{\partial a}, \\
\frac{d}{dt}\left(\frac{\partial r}{\partial a}\right) &= \frac{1}{\tau_I}\frac{\partial i}{\partial a}, \\
\frac{d}{dt}\left(\frac{\partial f}{\partial a}\right) &= \frac{1}{\tau_F}\left(\frac{\partial i}{\partial a} - \frac{\partial f}{\partial a}\right).
\end{aligned}$$

Sensitivity equations with respect to γ:

$$\begin{aligned}
\frac{d}{dt}\left(\frac{\partial s}{\partial \gamma}\right) &= \frac{\beta}{(1+af)^{\gamma}} si\ln(1+af) - \frac{\beta}{(1+af)^{\gamma}} i\frac{\partial s}{\partial \gamma} - \frac{\beta}{(1+af)^{\gamma}} s\frac{\partial i}{\partial \gamma} \\
&\quad + \frac{a\beta\gamma}{(1+af)^{\gamma+1}} si\frac{\partial f}{\partial \gamma}, \\
\frac{d}{dt}\left(\frac{\partial e}{\partial \gamma}\right) &= -\frac{\beta}{(1+af)^{\gamma}} si\ln(1+af) + \frac{\beta}{(1+af)^{\gamma}} i\frac{\partial s}{\partial \gamma} - \frac{1}{\tau_E}\frac{\partial e}{\partial \gamma} \\
&\quad + \frac{\beta}{(1+af)^{\gamma}} s\frac{\partial i}{\partial \gamma} - \frac{a\beta\gamma}{(1+af)^{\gamma+1}} si\frac{\partial f}{\partial \gamma}, \\
\frac{d}{dt}\left(\frac{\partial i}{\partial \gamma}\right) &= \frac{1}{\tau_E}\frac{\partial e}{\partial \gamma} - \frac{1}{\tau_I}\frac{\partial i}{\partial \gamma}, \\
\frac{d}{dt}\left(\frac{\partial r}{\partial \gamma}\right) &= \frac{1}{\tau_I}\frac{\partial i}{\partial \gamma}, \\
\frac{d}{dt}\left(\frac{\partial f}{\partial \gamma}\right) &= \frac{1}{\tau_F}\left(\frac{\partial i}{\partial \gamma} - \frac{\partial f}{\partial \gamma}\right).
\end{aligned}$$

C.4. Waning immunity, endogenous: SEIRSb

Sensitivity equations with respect to β:

$$\begin{aligned}
\frac{d}{dt}\left(\frac{\partial s}{\partial \beta}\right) &= -\frac{1}{(1+af)^{\gamma}} si - \frac{\beta}{(1+af)^{\gamma}} i\frac{\partial s}{\partial \beta} - \frac{\beta}{(1+af)^{\gamma}} s\frac{\partial i}{\partial \beta} + \frac{1}{\tau_r}\frac{\partial r}{\partial \beta} \\
&\quad + \frac{a\beta\gamma}{(1+af)^{\gamma+1}} si\frac{\partial f}{\partial \beta}, \\
\frac{d}{dt}\left(\frac{\partial e}{\partial \beta}\right) &= \frac{1}{(1+af)^{\gamma}} si + \frac{\beta}{(1+af)^{\gamma}} i\frac{\partial s}{\partial \beta} - \frac{1}{\tau_E}\frac{\partial e}{\partial \beta} \\
&\quad + \frac{\beta}{(1+af)^{\gamma}} s\frac{\partial i}{\partial \beta} - \frac{a\beta\gamma}{(1+af)^{\gamma+1}} si\frac{\partial f}{\partial \beta}, \\
\frac{d}{dt}\left(\frac{\partial i}{\partial \beta}\right) &= \frac{1}{\tau_E}\frac{\partial e}{\partial \beta} - \frac{i}{\tau_I}\frac{\partial I}{\partial \beta}, \\
\frac{d}{dt}\left(\frac{\partial r}{\partial \beta}\right) &= \frac{1}{\tau_I}\frac{\partial i}{\partial \beta} - \frac{1}{\tau_R}\frac{\partial r}{\partial \beta}, \\
\frac{d}{dt}\left(\frac{\partial f}{\partial \beta}\right) &= \frac{1}{\tau_F}\left(\frac{\partial i}{\partial \beta} - \frac{\partial f}{\partial \beta}\right).
\end{aligned}$$

Sensitivity equations with respect to a:

$$\begin{aligned}
\frac{d}{dt}\left(\frac{\partial s}{\partial a}\right) &= \frac{\beta\gamma f}{(1+af)^{\gamma+1}} si - \frac{\beta}{(1+af)^{\gamma}} i\frac{\partial s}{\partial a} - \frac{\beta}{(1+af)^{\gamma}} s\frac{\partial i}{\partial a} + \frac{1}{\tau_R}\frac{\partial r}{\partial a} \\
&\quad + \frac{a\beta\gamma}{(1+af)^{\gamma+1}} si\frac{\partial f}{\partial a}, \\
\frac{d}{dt}\left(\frac{\partial e}{\partial a}\right) &= -\frac{\beta\gamma f}{(1+af)^{\gamma+1}} si + \frac{\beta}{(1+af)^{\gamma}} i\frac{\partial s}{\partial a} - \frac{1}{\tau_E}\frac{\partial e}{\partial a} \\
&\quad + \frac{\beta}{(1+af)^{\gamma}} s\frac{\partial i}{\partial a} - \frac{a\beta\gamma}{(1+af)^{\gamma+1}} si\frac{\partial f}{\partial a}, \\
\frac{d}{dt}\left(\frac{\partial i}{\partial a}\right) &= \frac{1}{\tau_E}\frac{\partial e}{\partial a} - \frac{1}{\tau_I}\frac{\partial i}{\partial a}, \\
\frac{d}{dt}\left(\frac{\partial r}{\partial a}\right) &= \frac{1}{\tau_I}\frac{\partial i}{\partial a} - \frac{1}{\tau_R}\frac{\partial r}{\partial a}, \\
\frac{d}{dt}\left(\frac{\partial f}{\partial \alpha}\right) &= \frac{1}{\tau_F}\left(\frac{\partial i}{\partial a} - \frac{\partial f}{\partial a}\right).
\end{aligned}$$

Sensitivity equations with respect to γ:

$$\begin{aligned}
\frac{d}{dt}\left(\frac{\partial s}{\partial \gamma}\right) &= \frac{\beta}{(1+af)^{\gamma}} si\ln(1+af) - \frac{\beta}{(1+af)^{\gamma}} i\frac{\partial s}{\partial \gamma} - \frac{\beta}{(1+af)^{\gamma}} s\frac{\partial i}{\partial \gamma} \\
&\quad + \frac{1}{\tau_R}\frac{\partial r}{\partial \gamma} + \frac{a\beta\gamma}{(1+af)^{\gamma+1}} si\frac{\partial f}{\partial \gamma}, \\
\frac{d}{dt}\left(\frac{\partial e}{\partial \gamma}\right) &= -\frac{\beta}{(1+af)^{\gamma}} si\ln(1+af) + \frac{\beta}{(1+af)^{\gamma}} i\frac{\partial s}{\partial \gamma} - \frac{1}{\tau_E}\frac{\partial e}{\partial \gamma} \\
&\quad + \frac{\beta}{(1+af)^{\gamma}} s\frac{\partial i}{\partial \gamma} - \frac{a\beta\gamma}{(1+af)^{\gamma+1}} si\frac{\partial f}{\partial \gamma}, \\
\frac{d}{dt}\left(\frac{\partial i}{\partial \gamma}\right) &= \frac{1}{\tau_E}\frac{\partial e}{\partial \gamma} - \frac{1}{\tau_I}\frac{\partial i}{\partial \gamma}, \\
\frac{d}{dt}\left(\frac{\partial r}{\partial \gamma}\right) &= \frac{1}{\tau_I}\frac{\partial i}{\partial \gamma} - \frac{1}{\tau_R}\frac{\partial r}{\partial \gamma}, \\
\frac{d}{dt}\left(\frac{\partial f}{\partial \gamma}\right) &= \frac{1}{\tau_F}\left(\frac{\partial i}{\partial \gamma} - \frac{\partial f}{\partial \gamma}\right).
\end{aligned}$$

Sensitivity equations with respect to τ_R:

$$\begin{aligned}
\frac{d}{dt}\left(\frac{\partial s}{\partial \tau_R}\right) &= -\frac{r}{\tau_R^2} - \frac{\beta}{(1+af)^{\gamma}} i\frac{\partial s}{\partial \tau_R} - \frac{\beta}{(1+af)^{\gamma}} s\frac{\partial i}{\partial \tau_R} + \frac{1}{\tau_R}\frac{\partial r}{\partial \tau_R} \\
&\quad + \frac{a\beta\gamma}{(1+af)^{\gamma+1}} si\frac{\partial f}{\partial \tau_R}, \\
\frac{d}{dt}\left(\frac{\partial e}{\partial \tau_R}\right) &= \frac{\beta}{(1+af)^{\gamma}} i\frac{\partial s}{\partial \tau_R} - \frac{1}{\tau_E}\frac{\partial e}{\partial \tau_R} \\
&\quad + \frac{\beta}{(1+af)^{\gamma}} s\frac{\partial i}{\partial \tau_R} - \frac{a\beta\gamma}{(1+af)^{\gamma+1}} si\frac{\partial f}{\partial \tau_R}, \\
\frac{d}{dt}\left(\frac{\partial i}{\partial \tau_R}\right) &= \frac{1}{\tau_E}\frac{\partial e}{\partial \tau_R} - \frac{1}{\tau_I}\frac{\partial i}{\partial \tau_R}, \\
\frac{d}{dt}\left(\frac{\partial r}{\partial \tau_R}\right) &= \frac{r}{\tau_R^2} + \frac{1}{\tau_I}\frac{\partial i}{\partial \tau_R} - \frac{1}{\tau_R}\frac{\partial r}{\partial \tau_R}, \\
\frac{d}{dt}\left(\frac{\partial f}{\partial \tau_R}\right) &= \frac{1}{\tau_F}\left(\frac{\partial i}{\partial \tau_R} - \frac{\partial f}{\partial \tau_R}\right).
\end{aligned}$$

To clarify the time-varying sensitivity and semi-relative sensitivity results found in Fig. 4, we show dynamics of the infectious population for various choices of β, a, γ, and τ_R, as well as for parameters not considered in the time-varying sensitivity analysis (τ_E, τ_I, and τ_F) in Fig. C.1. We do not show SEIRb model solutions as Figs. C.1(a)–C.1(f) are visually identical between the SEIRb and SEIRSb models and τ_R is not included in the SEIRb model. As β increases, the infectious population exhibits higher values, while as a and γ increase, the infectious population obtains lower values. This is due to the placement of β in the numerator of the transmission term and a and γ in the denominator. With respect to changes in β, the difference in solutions increases for the first 30 days as the solutions approach the peak of the first oscillation. Following the peak, the difference in solutions then decreases as solutions approach the first trough (at about day 75), increasing again after the trough for about 50 days until the next peak. This pattern continues, with the difference between solution sizes approaching a constant value as oscillations dampen. There is similar behavior in the difference in solutions with respect to changes in a (Fig. C.1(b)) and γ (C.1(c)). Notably, as these two parameters increase, the magnitude of solutions decreases, in contrast to β, and

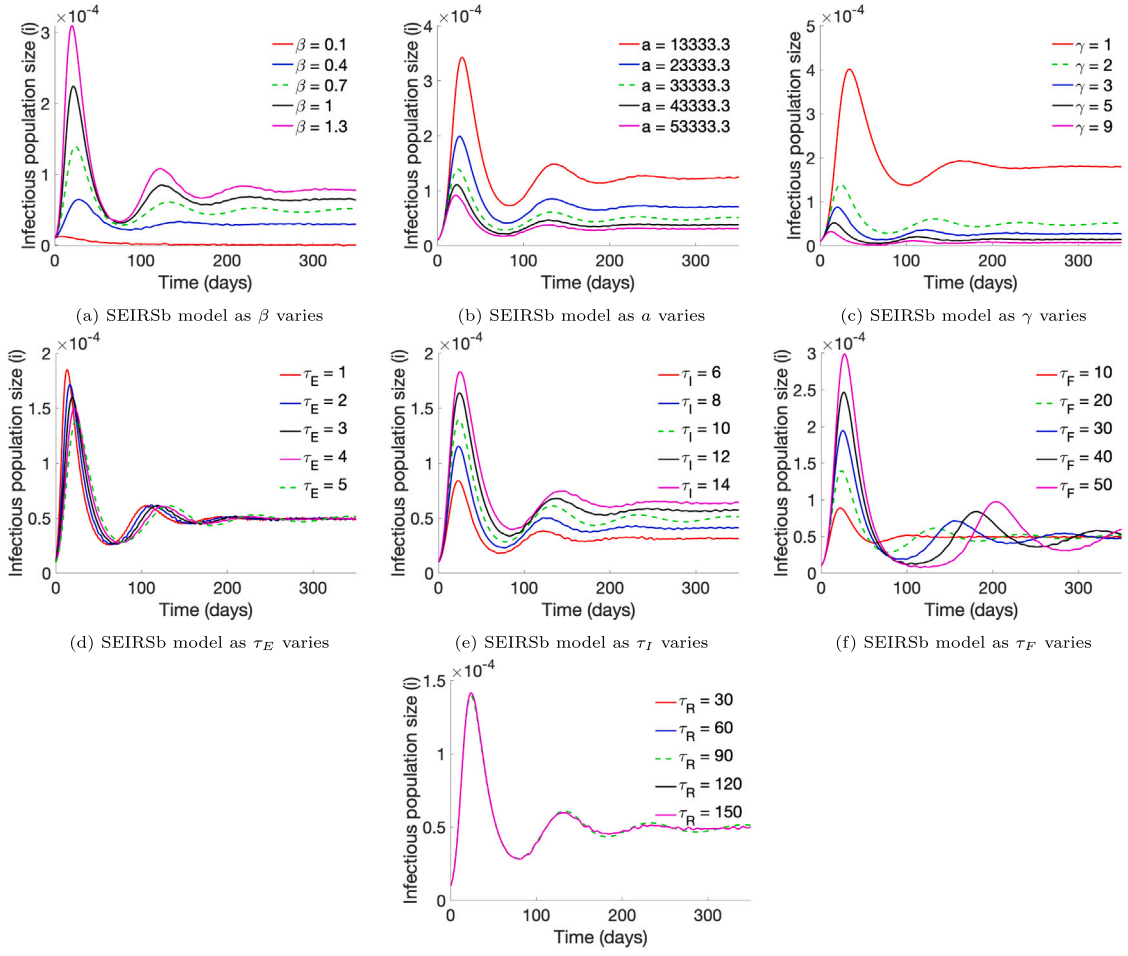

(a) SEIRSb model as β varies (b) SEIRSb model as a varies (c) SEIRSb model as γ varies

(d) SEIRSb model as τ_E varies (e) SEIRSb model as τ_I varies (f) SEIRSb model as τ_F varies

(g) SEIRSb model as τ_R varies

Fig. C.1. SEIRSb model solutions for differing values of (a) β, (b) a, (c) γ, (d) τ_E, (e) τ_I, (f) τ_F, and (g) τ_R. Standard parameter values are shown with a dashed line. Note that all lines can be found in (g) but as τ_R does not appreciably affect the model solution in the first 350 days, the lines lie on top of each other. We do not show SEIRb model solutions as (a)–(f) are visually identical between the SEIRb and SEIRSb models and τ_R is not included in the SEIRb model.

correspondingly, the sensitivities for β are positive but are negative for a and γ (Fig. 4). Furthermore, the difference between solutions significantly decreases as these two parameters increase. Solutions show little change with respect to changes in τ_R, indicating that solutions for the SEIRSb infectious population size i are not sensitive to changes in the period of immunity, at least across the first 350 days.

To aid in interpretation of the global sensitivity results (Fig. 5), we also show dynamics of the infectious population for various choices of τ_E, τ_I, and τ_F (Figs. C.1(d)–C.1(f)). Increases in τ_E result in a decrease in solution magnitude and a delay in peak occurrence of the first and subsequent peaks. In contrast, increases in τ_I result in increases in solution magnitude and a slight delay in peak timing as well as clear increases in the endemic equilibrium. Increases in τ_F result in stronger oscillatory behavior: solutions have higher, wider peaks and lower, wider troughs. Furthermore, oscillatory behavior lasts longer before dampening to the equilibrium.

Lastly, we clarify our choice of parameter values for Figs. 3 and C.1. The choice of parameters is based on the values listed in Table 4. Perturbations of a fixed size were chosen for each parameter (for example, all values of β differ by 0.3) to display an assortment of values that falls within the range given in Table 4. The exception here is parameter γ, where the value of $\gamma = 9$ is included to show the negligible difference between $\gamma = 5$ and $\gamma = 9$. This supports the choice of $\gamma = 5$ as the upper bound for the range of γ values.

Appendix D. Methods for model validation

For data replication, we use data from [56]. The model formulation is similar to that described in the main text using the modified scaled models, based on Systems (2) and (4). For model validation of models with human behavior, we use the following for the SEIRb and SEIRb with seasonality

$$\begin{aligned}
\frac{ds_j}{dt} &= -\frac{\beta_j}{(1+a_j f_j)^{\gamma_j}}\theta_j s_j i_j,\\
\frac{de_j}{dt} &= \frac{\beta_j}{(1+a_j f_j)^{\gamma_j}}\theta_j s_j i_j - \frac{e_j}{\tau_E},\\
\frac{di_j}{dt} &= \frac{e_j}{\tau_E} - \frac{i_j}{\tau_I},\\
\frac{dr_j}{dt} &= (1-IFR)\frac{i_j}{\tau_I},\\
\frac{df_j}{dt} &= \frac{i_j - f_j}{\tau_F},
\end{aligned} \tag{D.1}$$

and the following for the SEIRSb and SEIRSb with seasonality

$$\begin{aligned}
\frac{ds_j}{dt} &= -\frac{\beta_j}{(1+a_j f_j)^{\gamma_j}}\theta_j s_j i_j + \frac{r_j}{\tau_R},\\
\frac{de_j}{dt} &= \frac{\beta_j}{(1+a_j f_j)^{\gamma_j}}\theta_j s_j i_j - \frac{e_j}{\tau_E},
\end{aligned}$$

Table D.1
Parameters estimated for each model when fitting to US region data. Note that c_0, the fitted time of the appearance of case zero in the region, and w, the size of the seasonal effect, are not found in our original model. Parameters not found below in the table are fixed to their standard values: $\tau_E = 5$ and $\tau_I = 10$. Initial conditions are $s(c_0) = 1$, $e(c_0) = 10^{-6}$, $i(c_0) = r(c_0) = f(c_0) = 0$. For each region, model output d_j, described in Eq. (D.6), was fitted to each region's daily per capita death per million. For illustrative purposes in Figs. 7 and D.3, simulation output and data were scaled to the population size for each region.

Parameter	Range	Local vs. global	Models SEIRS	SEIRS with seasonality	SEIRSb	SEIRb with seasonality	SEIRSb with seasonality
β	$[0.15, 0.7]$	Local	Yes	Yes	Yes	Yes	Yes
γ	$[0, 4]$	Local			Yes	Yes	Yes
α	$[0, 0.01]$	Local			Yes	Yes	Yes
τ_F	$[7, 200]$	Local			Yes	Yes	Yes
τ_R	$[60, 365]$	Global	Yes	Yes	Yes		Yes
c_0	$[0, 120]$	Local	Yes	Yes	Yes	Yes	Yes
w	$[0, 1]$	Local		Yes		Yes	Yes

Table D.2
Model performance (R-squared) in replicating different US region data.

US region	SEIRS	SEIRS with seasonality	SEIRSb	SEIRb with seasonality	SEIRSb with seasonality
Alabama	0.61	0.61	0.68	0.79	0.80
Alaska	0.01	0.01	0.49	0.48	0.49
Arizona	0.57	0.57	0.35	0.59	0.77
Arkansas	0.63	0.63	0.67	0.74	0.74
California	0	0.01	0.83	0.90	0.90
Colorado	0.02	0.02	0.43	0.83	0.83
Connecticut	0.03	0.03	0.96	0.97	0.97
Delaware	0.02	0.02	0.72	0.84	0.85
District of Columbia	0.02	0.03	0.94	0.95	0.95
Florida	0	0	0.70	0.82	0.84
Georgia	0	0	0.34	0.49	0.51
Hawaii	0	0.01	0.29	0.41	0.41
Idaho	0.02	0.03	0.82	0.85	0.85
Illinois	0.03	0.04	0.48	0.96	0.96
Indiana	0.71	0.71	0.83	0.94	0.94
Iowa	0.02	0.03	0.64	0.68	0.68
Kansas	0.74	0.74	0.79	0.81	0.82
Kentucky	0.03	0.03	0.53	0.54	0.54
Louisiana	0.08	0.10	0.64	0.71	0.68
Maine	0	0	0.69	0.75	0.75
Maryland	0.02	0	0.62	0.65	0.67
Massachusetts	0.03	0.03	0.91	0.92	0.91
Michigan	0.01	0.01	0.65	0.78	0.79
Minnesota	0.01	0.02	0.27	0.92	0.92
Mississippi	0.43	0.43	0.35	0.73	0.75
Missouri	0.01	0.02	0.76	0.80	0.80
Montana	0	0	0.75	0.78	0.77
Nebraska	0.04	0.04	0.80	0.85	0.85
Nevada	0.02	0.03	0.78	0.78	0.82
New Hampshire	0	0.01	0.43	0.90	0.90
New Jersey	0.02	0.01	0.96	0.97	0.96
New Mexico	0.77	0.77	0.87	0.88	0.89
New York	0.01	0.01	0.96	0.97	0.96
North Carolina	0	0.01	0.71	0.84	0.84
North Dakota	0.86	0.86	0.90	0.91	0.91
Ohio	0.76	0.76	0.91	0.97	0.97
Oklahoma	0.05	0.10	0.18	0.19	0.19
Oregon	0	0	0.74	0.74	0.74
Pennsylvania	0.54	0.54	0.40	0.93	0.93
Rhode Island	0.28	0.28	0.71	0.95	0.96
South Carolina	0.01	0.02	0.46	0.68	0.67
South Dakota	0.86	0.86	0.93	0.94	0.94
Tennessee	0.71	0.71	0.78	0.85	0.84
Texas	0.01	0.02	0.54	0.81	0.85
Utah	0	0.01	0.84	0.89	0.87
Vermont	0	0	0.33	0.86	0.86
Virginia	0	0	0.13	0.28	0.28
Washington	0	0.01	0.33	0.63	0.66
West Virginia	0	0.01	0.69	0.69	0.69
Wisconsin	0.01	0.02	0.87	0.88	0.88
Wyoming	0.70	0.70	0.85	0.86	0.86

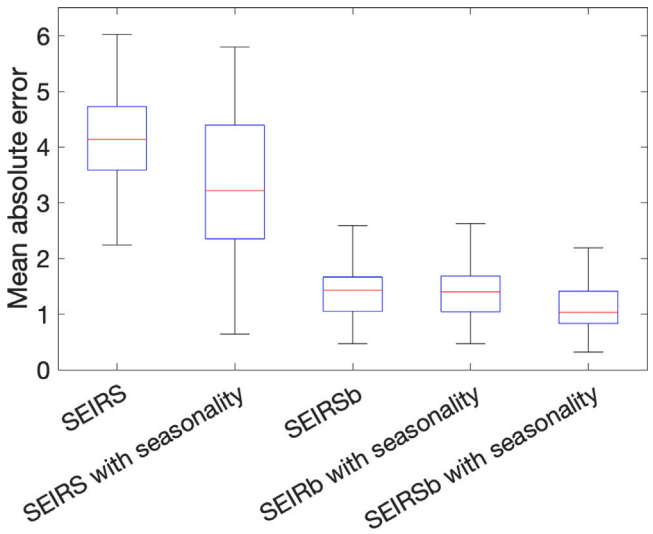

Fig. D.1. Distribution of mean absolute error of 5 different models across 51 US regions. Red line is the median, blue box is 25%–75% percentile, and whiskers represent the 95% interval.

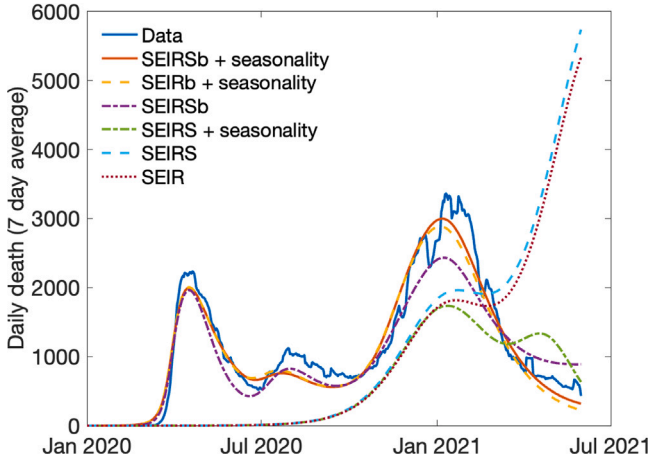

Fig. D.2. Comparisons of fits of each model (SEIRSb + seasonality, SEIRb + seasonality, SEIRSb, SEIRS + seasonality, SEIRS, SEIR) for all US data. All US graphs are generated after fitting each state simulation to its corresponding data. Note we also include the exogenous SEIR and SEIRS models with fixed base transmission rate, β, for comparison.

$$\begin{aligned}\frac{di_j}{dt} &= \frac{e_j}{\tau_E} - \frac{i_j}{\tau_I},\\ \frac{dr_j}{dt} &= (1-IFR)\frac{i_j}{\tau_I} - \frac{r_j}{\tau_R},\\ \frac{df_j}{dt} &= \frac{i_j - f_j}{\tau_F},\end{aligned} \tag{D.2}$$

where j is the index for the US region, IFR is the infection fatality rate, θ_j incorporates seasonality (described below) and other parameters are found in Table D.1.

The variable θ is added to include seasonality. We intentionally use a simple sinusoidal equation given by

$$\theta_j = 1 + w_j \sin\left(\frac{2\pi(t+91)}{365}\right), \tag{D.3}$$

where t is time (in days) since January 1st, 2020, and $0 \le w_j \le 1$ is the size of seasonal effect, which is estimated through model calibration for each US region. The shift in the sinusoidal function by 91/365 (about one quarter of a year) is used to adjust the phase such that its maximum value occurs on January 1st. Based on Eq. (D.3), then $1-w \le \theta \le 1+w$, and for $w = 0$, then $\theta(t) = 1$, representing no seasonality effect.

For the models without human behavior (SEIRS and SEIRS with seasonality), we use the following

$$\begin{aligned}\frac{ds_j}{dt} &= -\beta_j\theta_j s_j i_j + \frac{r_j}{\tau_R},\\ \frac{de_j}{dt} &= \beta_j\theta_j s_j i_j - \frac{e_j}{\tau_E},\\ \frac{di_j}{dt} &= \frac{e_j}{\tau_E} - \frac{i_j}{\tau_I},\\ \frac{dr_j}{dt} &= (1-IFR)\frac{i_j}{\tau_I} - \frac{r_j}{\tau_R},\end{aligned} \tag{D.4}$$

where j is the index for the US region, IFR is the infection fatality rate, and other parameters are found in Table D.1. In the case without seasonality (SEIRS), $\theta_j = 1$, while with seasonality, θ_j is the same as in Eq. (D.3). Note that as there is no feedback into the base transmission rate, such that β_j is a constant for each region. There is no need for the state variable f in these models as f does not feedback on other variables.

For the models without human behavior (SEIR and SEIR with seasonality), we use the following

$$\begin{aligned}\frac{ds_j}{dt} &= -\beta_j\theta_j s_j i_j,\\ \frac{de_j}{dt} &= \beta_j\theta_j s_j i_j - \frac{e_j}{\tau_E},\\ \frac{di_j}{dt} &= \frac{e_j}{\tau_E} - \frac{i_j}{\tau_I},\\ \frac{dr_j}{dt} &= (1-IFR)\frac{i_j}{\tau_I},\end{aligned} \tag{D.5}$$

where j is the index for the US region. In the case without seasonality (SEIR), $\theta_j = 1$, while with seasonality, θ_j is the same as in Eq. (D.3). Similar to the SEIR model, as there is no feedback into the base transmission rate, such that β_j is a constant for each region, there is no need for the state variable f in these models.

For model calibration we estimate parameters to maximize the fit between the simulation and data for each US region by minimizing the mean square error using daily death data (per capita) per million. As mentioned in Section 4.4, in the model, we calculate daily per capita death, d_j, as

$$d_j = IFR\left(\frac{i_j}{\tau_I}\right), \tag{D.6}$$

where j is the index for the US region (50 states and District of Columbia) and IFR is the infection fatality rate, which we assume is 0.5% [54]. The parameters fitted for each model are found in Table D.1.

Performance of the five models in replicating overall US data are reported in Table 5, Figs. 6 and D.1. The final model performance in replicating each of the 51 US regions is reported in Table D.2 and Fig. D.3.

Appendix E. Supplementary data

Supplementary material related to this article can be found online at https://doi.org/10.1016/j.mbs.2024.109250.

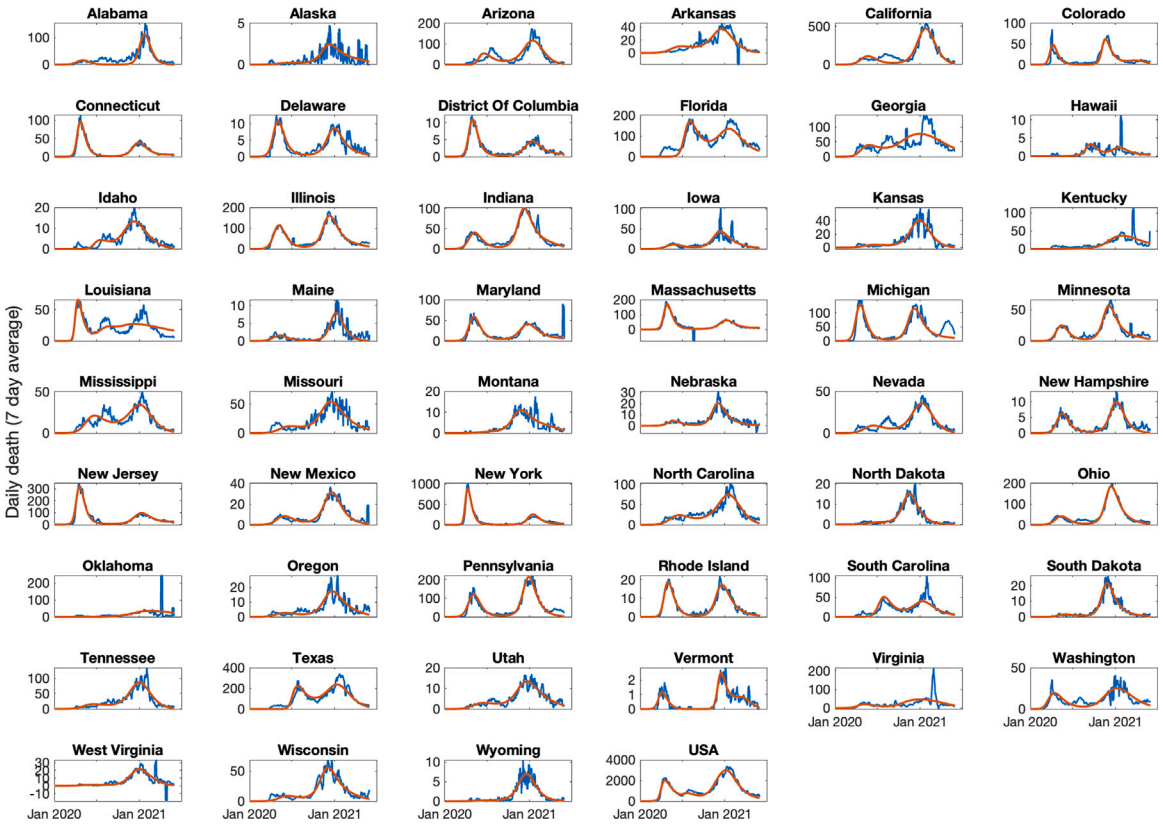

Fig. D.3. Simulation results against data for daily death per capita per million in 51 US regions as well as the entire country. Blue lines are data, and red lines are model outcome. Note: The y-axis differs for each region. Some states have daily death below zero because of corrections to the data.

References

[1] J. Panovska-Griffiths, C. Kerr, W. Waites, R. Stuart, Mathematical modeling as a tool for policy decision making: Applications to the COVID-19 pandemic, in: Handbook of Statistics, Vol. 44, Elsevier, 2021, pp. 291–326.

[2] J. Koffman, J. Gross, S.N. Etkind, L. Selman, Uncertainty and COVID-19: how are we to respond? J. R. Soc. Med. 113 (6) (2020) 211–216.

[3] J. Zhang, How did people respond to the COVID-19 pandemic during its early stage? A case study in Japan, 2020.

[4] H. Rahmandad, R. Xu, N. Ghaffarzadegan, Enhancing long-term forecasting: Learning from COVID-19 models, PLoS Comput. Biol. 18 (5) (2022) e1010100.

[5] W.O. Kermack, A.G. McKendrick, A contribution to the mathematical theory of epidemics, Proc. R. Soc. A 115 (772) (1927) 700–721.

[6] R.M. Anderson, R.M. May, Infectious Diseases of Humans: Dynamics and Control, Oxford University Press, 1991.

[7] M. Martcheva, An Introduction to Mathematical Epidemiology, Vol. 61, Springer, 2015.

[8] Y. Pan, A. Darzi, A. Kabiri, G. Zhao, W. Luo, C. Xiong, et al., Quantifying human mobility behaviour changes during the COVID-19 outbreak in the United States, Sci. Rep. 10 (1) (2020) 20742.

[9] D.W. Dick, L. Childs, Z. Feng, J. Li, G. Röst, D.L. Buckeridge, et al., COVID-19 seroprevalence in Canada modelling waning and boosting COVID-19 immunity in Canada a Canadian immunization research network study, Vaccines 10 (1) (2021) 17.

[10] K.M. Bubar, K. Reinholt, S.M. Kissler, M. Lipsitch, S. Cobey, Y.H. Grad, et al., Model-informed COVID-19 vaccine prioritization strategies by age and serostatus, Science 371 (6352) (2021) 916–921.

[11] S. Dryhurst, C.R. Schneider, J. Kerr, A.L. Freeman, G. Recchia, A.M. Van Der Bles, et al., Risk perceptions of COVID-19 around the world, in: COVID-19, Routledge, 2022, pp. 162–174.

[12] D. Tsoy, T. Tirasawasdichai, K.I. Kurpayanidi, et al., Role of social media in shaping public risk perception during COVID-19 pandemic: A theoretical review, Int. J. Manag. Sci. Bus. Adm. 7 (2) (2021) 35–41.

[13] S. Funk, M. Salathé, V.A. Jansen, Modelling the influence of human behaviour on the spread of infectious diseases: a review, J. R. Soc. Interface 7 (50) (2010) 1247–1256.

[14] N. Perra, Non-pharmaceutical interventions during the COVID-19 pandemic: A review, Phys. Rep. 913 (2021) 1–52.

[15] N. Ghaffarzadegan, Simulation of the spread of COVID-19 at virginia tech, in: Proceedings of the IISE Annual Conference & Expo 2022, Seattle, WA, 2022.

[16] Z. Qiu, B. Espinoza, V.V. Vasconcelos, C. Chen, S.M. Constantino, S.A. Crabtree, et al., Understanding the coevolution of mask wearing and epidemics: A network perspective, Proc. Natl. Acad. Sci. 119 (26) (2022) e2123355119.

[17] V. d'Andrea, R. Gallotti, N. Castaldo, M. De Domenico, Individual risk perception and empirical social structures shape the dynamics of infectious disease outbreaks, PLoS Comput. Biol. 18 (2) (2022) e1009760.

[18] J.C. Miller, E.M. Volz, Incorporating disease and population structure into models of SIR disease in contact networks, PLoS One 8 (8) (2013) e69162.

[19] X. Hong, Y. Han, B. Wang, Impacts of self-initiated behavioral responses and pandemic fatigue on the epidemic spread in time-varying multiplex networks, Chaos Solitons Fractals 173 (2023) 113696.

[20] F.B. Agusto, I.V. Erovenko, A. Fulk, Q. Abu-Saymeh, D. Romero-Alvarez, J. Ponce, et al., To isolate or not to isolate: the impact of changing behavior on COVID-19 transmission, BMC Public Health 22 (1) (2022) 138.

[21] B. Espinoza, S. Swarup, C.L. Barrett, M. Marathe, Heterogeneous adaptive behavioral responses may increase epidemic burden, Sci. Rep. 12 (1) (2022) 11276.

[22] J. Cascante-Vega, S. Torres-Florez, J. Cordovez, M. Santos-Vega, How disease risk awareness modulates transmission: coupling infectious disease models with behavioural dynamics, Royal Soc. Open Sci. 9 (1) (2022) 210803.

[23] C.M. Saad-Roy, A. Traulsen, Dynamics in a behavioral–epidemiological model for individual adherence to a nonpharmaceutical intervention, Proc. Natl. Acad. Sci. 120 (44) (2023) e2311584120.

[24] K. Peng, Z. Lu, V. Lin, M.R. Lindstrom, C. Parkinson, C. Wang, et al., A multilayer network model of the coevolution of the spread of a disease and competing opinions, Math. Models Methods Appl. Sci. 31 (12) (2021) 2455–2494.

[25] R.C. Tyson, S.D. Hamilton, A.S. Lo, B.O. Baumgaertner, S.M. Krone, The timing and nature of behavioural responses affect the course of an epidemic, Bull. Math. Biol. 82 (2020) 1–28.

[26] E. Yedomonhan, C.F. Tovissodé, R.G. Kakaï, Modeling the effects of prophylactic behaviors on the spread of SARS-CoV-2 in West Africa, Math. Biosci. Eng. 20 (7) (2023) 12955–12989.

[27] B. Morsky, F. Magpantay, T. Day, E. Akçay, The impact of threshold decision mechanisms of collective behavior on disease spread, Proc. Natl. Acad. Sci. 120 (19) (2023) e2221479120.

[28] J.S. Weitz, S.W. Park, C. Eksin, J. Dushoff, Awareness-driven behavior changes can shift the shape of epidemics away from peaks and toward plateaus, shoulders, and oscillations, Proc. Natl. Acad. Sci. 117 (51) (2020) 32764–32771.

[29] J. Sooknanan, T.A. Seemungal, FOMO (fate of online media only) in infectious disease modeling: a review of compartmental models, Int. J. Dyn. Control 11 (2) (2023) 892–899.
[30] F. Verelst, L. Willem, P. Beutels, Behavioural change models for infectious disease transmission: a systematic review (2010–2015), J. R. Soc. Interface 13 (125) (2016) 20160820.
[31] A. Hamilton, F. Haghpanah, A. Tulchinsky, N. Kipshidze, S. Poleon, G. Lin, et al., Incorporating endogenous human behavior in models of COVID-19 transmission: A systematic scoping review, Dialogues Health (2024) 100179.
[32] L. LeJeune, N. Ghaffarzadegan, L. Childs, O. Saucedo, Formulating human risk response in epidemic models: exogenous vs endogenous approaches, 2024, arXiv preprint arXiv:240515535.
[33] H. Rahmandad, R. Xu, N. Ghaffarzadegan, A missing behavioural feedback in COVID-19 models is the key to several puzzles, BMJ Global Health 7 (10) (2022) e010463.
[34] A. Osi, N. Ghaffarzadegan, Parameter estimation in behavioral epidemic models with endogenous societal risk-response, PLoS Comput. Biol. 20 (3) (2024) e1011992.
[35] J.P.N. N'konzi, C.W. Chukwu, F. Nyabadza, Effect of time-varying adherence to non-pharmaceutical interventions on the occurrence of multiple epidemic waves: A modeling study, Front. Public Health 10 (2022) 1087683.
[36] W. Abbas, M.A. M, A. Park, S. Parveen, S. Kim, Evolution and consequences of individual responses during the COVID-19 outbreak, PLoS One 17 (9) (2022) e0273964.
[37] T. Li, Y. Xiao, Complex dynamics of an epidemic model with saturated media coverage and recovery, Nonlinear Dynam. (2022) 1–29.
[38] J.C. Blackwood, L.M. Childs, An introduction to compartmental modeling for the budding infectious disease modeler, Letters in Biomathematics (2018).
[39] P. Van den Driessche, J. Watmough, Reproduction numbers and sub-threshold endemic equilibria for compartmental models of disease transmission, Math. Biosci. 180 (1–2) (2002) 29–48.
[40] O. Diekmann, J.A.P. Heesterbeek, Mathematical Epidemiology of Infectious Diseases: Model Building, Analysis and Interpretation. Vol. 5, John Wiley & Sons, 2000.
[41] M. Bani-Yaghoub, R. Gautam, Z. Shuai, P. Van Den Driessche, R. Ivanek, Reproduction numbers for infections with free-living pathogens growing in the environment, J. Biol. Dyn. 6 (2) (2012) 923–940.
[42] N. Meshkat, S. Sullivant, M. Eisenberg, Identifiability results for several classes of linear compartment models, Bull. Math. Biol. 77 (2015) 1620–1651.
[43] O. Saucedo, A. Laubmeier, T. Tang, B. Levy, L. Asik, T. Pollington, et al., Comparative analysis of practical identifiability methods for an SEIR model, 2024, arXiv preprint arXiv:240115076.
[44] N. Tuncer, T.T. Le, Structural and practical identifiability analysis of outbreak models, Math. Biosci. 299 (2018) 1–18.
[45] H. Miao, X. Xia, A.S. Perelson, H. Wu, On identifiability of nonlinear ODE models and applications in viral dynamics, SIAM Rev. 53 (1) (2011) 3–39.
[46] M.C. Eisenberg, M.A. Hayashi, Determining identifiable parameter combinations using subset profiling, Math. Biosci. 256 (2014) 116–126.
[47] X. Rey Barreiro, A.F. Villaverde, Benchmarking tools for a priori identifiability analysis, Bioinformatics 39 (2) (2023) btad065.
[48] R. Dong, C. Goodbrake, H.A. Harrington, G. Pogudin, Differential elimination for dynamical models via projections with applications to structural identifiability, SIAM J. Appl. Algebra Geom. 7 (1) (2023) 194–235.
[49] S.A. Lauer, K.H. Grantz, Q. Bi, F.K. Jones, Q. Zheng, H.R. Meredith, et al., The incubation period of coronavirus disease 2019 (COVID-19) from publicly reported confirmed cases: estimation and application, Ann. Intern. Med. 172 (9) (2020) 577–582.
[50] Centers for Disease Control and Prevention 2023, Centers for disease control and prevention, 2023, Available from: https://www.cdc.gov/coronavirus/2019-ncov/hcp/duration-isolation.html.
[51] D.S. Stephens, M.J. McElrath, COVID-19 and the path to immunity, JAMA 324 (13) (2020) 1279–1281.
[52] A. Razdan, R. Arora, G. Agarwal, V. Sharma, N. Singh, J. Kandpal, et al., COVID-19 pandemic to endemic, Int. J. Clin. Virol. 6 (2) (2022) 043–049.
[53] S. Marino, I.B. Hogue, C.J. Ray, D.E. Kirschner, A methodology for performing global uncertainty and sensitivity analysis in systems biology, J. Theoret. Biol. 254 (1) (2008) 178–196.
[54] J.S. Faust, C. Del Rio, Assessment of deaths from COVID-19 and from seasonal influenza, JAMA Internal Med. 180 (8) (2020) 1045–1046.
[55] H. Rahmandad, T.Y. Lim, J. Sterman, Behavioral dynamics of COVID-19: estimating underreporting, multiple waves, and adherence fatigue across 92 nations, Syst. Dyn. Rev. 37 (1) (2021) 5–31.
[56] E. Dong, H. Du, L. Gardner, An interactive web-based dashboard to track COVID-19 in real time, Lancet Infect. Dis. 20 (5) (2020) 533–534.